A cost-effective approach for comprehensive analysis of human memory B Cell repertoire: fast isolation of broad neutralizing mAbs to SARS-CoV-2 variants

Luciana Conde [1,2,#], Debora L. Oliveira[1,#], Gabriela Maciel[1], Fernando Castro[1], Aline de Oliveira Albuquerque[3], Danielle Rodrigues[1], Gustavo Meira[1,4], Bárbara Gabrielle[1], Suyane S. Ferreira[5], Marcela S. Cunha[5], Carlena Navas[6], Manuela C. Emiliano [6], Marcele N. Rocha[6], Barbara Soares[1], Lucas Tostes[1], Yare Mello[1], Phillippe Caloba[1], Bruno Maia[5], Amilcar Tanuri[7], Orlando Ferreira[7], Terezinha Castineiras[8], Juliana Echevarria[5], Marcelo Bozza[5], João Hermínio Martins da Silva[3], Alberto Nobrega[5], Leda Castilho[9], Liza F. Felicori[6], Luciana J. da Costa[8], Gabriel Victora[4], Carolina Lucas[2], Adriana Bonomo[10], André M. Vale[1,*]

[1] Laboratório de Biologia de Linfócitos, Instituto de Biofísica Carlos Chagas Filho, Universidade Federal do Rio de Janeiro, Rio de Janeiro, RJ, Brazil.

[2] Department of Immunobiology, Yale University School of Medicine, New Haven, CT, USA

[3] Fundação Oswaldo Cruz. FIOCRUZ Ceará. Eusébio, CE, Brazil.

[4] Laboratory of Lymphocyte Dynamics, The Rockefeller University, New York, NY, USA

[5] Instituto de Microbiologia Paulo de Góes, Universidade Federal do Rio de Janeiro, Rio de Janeiro, Brazil.

[6] Laboratory of Synthetic Biology and Biomimetics, Departamento de Bioquímica e Imunologia, Instituto de Ciências Biológicas - ICB, Universidade Federal de Minas Gerais, Belo Horizonte, Brazil

[7] Laboratório de Virologia Molecular, Departamento de Genética, Instituto de Biologia, Universidade Federal do Rio de Janeiro, Rio de Janeiro, RJ, Brasil

[8] Núcleo de Enfrentamento e Estudos de Doenças Infecciosas Emergentes e Reemergentes, Universidade Federal do Rio de Janeiro, Rio de Janeiro, RJ, Brasil

[9] Programa de Engenharia Química, Laboratório de Engenharia de Cultivos Celulares (LECC), COPPE, Universidade Federal do Rio de Janeiro, Rio de Janeiro, 21941-972, Brazil.

[10] Thymus Research Laboratory , Fundação Oswaldo Cruz, IOC-FIOCRUZ, Rio de Janeiro, Brazil

[#]These authors contributed equally.

*Correspondence to André M. Vale: valeam@biof.ufrj.br

Abstract

The SARS-CoV-2 pandemic highlighted the urgent need for innovative methods to study humoral immune responses and identify monoclonal antibodies (mAbs) with diagnostic and therapeutic potential. Memory B cells (MBCs), pivotal to adaptive immunity, generate high-affinity antibodies upon antigen re-encounter. While single-cell high-throughput sequencing has revolutionized antibody repertoire studies, it has critical limitations: the inability to simultaneously determine antigen-binding specificities and immunoglobulin gene sequences, and high resource demands that limit accessibility in low-resource settings. Here, we present a cost-effective single-cell culture (SCC) platform enabling comprehensive analysis of human MBC repertoires, including epitope-specific responses, cross-reactivity studies, and mAb isolation. Using SARS-CoV-2 convalescent and vaccinated donor samples, we optimized MBC SCCs with NB21 feeder cells, R848, and IL-2 stimulation, achieving high cloning efficiency and a 30-fold enrichment of antigen-specific MBCs compared to bulk cultures. Among 592 isolated mAbs, 52.7% exhibited specificity to the Wuhan strain Spike protein, with 27.9% targeting the receptor-binding domain (RBD), 15.4% the N-terminal domain (NTD), and 56.7% other regions, likely the S2 domain. Comparative analysis revealed distinct cross-reactivity patterns: 40.5% of all anti-Spike mAbs recognized all tested SARS-CoV-2 variants (Wuhan, Beta, Delta, Gamma and Omicron BA.2), while 29.6% showed recognition of only four variants, the majority not including Omicron BA.2; 56 single strain reactive mAbs (14.9%) were also identified. Notably, all screening and neutralization assays were performed directly with culture supernatants, eliminating the need for large-scale sequencing and transfection. Desired clones were selected for recombinant mAb production. The SCC platform also enabled unbiased immunoglobulin repertoire profiling, revealing convergent V-region rearrangements, including public V3-30 and V3-53/V3-66 antibodies consistent with prior SARS-CoV-2 studies. Two public RBD-targeting clones with broad neutralization potential were validated in pseudovirus neutralization assays. This streamlined platform delivers simultaneous antigen-specific mAb isolation, V-region sequencing, and functional studies within seven days, empowering researchers in low-resource settings to address global health inequities and enhance preparedness for future pandemics.

Introduction

The SARS-CoV-2 pandemic, with its high morbidity and mortality rates [1], underscored an urgent need for new methods to study and monitor the humoral immune response to infection and vaccination at the level of individual B cell clonotypes. Immune escape during the pandemic occurred through the accumulation of mutations in the viral genome, leading to highly transmissible Variants of Concern (VOCs) and significant antigenic drift in the Spike protein. These mutations, concentrated primarily in the receptor-binding domain (RBD) and the N-terminal domain (NTD), posed challenges to vaccination strategies and emphasized the need of vaccine generated cross-reactive and broadly neutralizing antibody responses [2].

Memory B cells (MBCs) are essential components of the adaptive immune response, playing a critical role in long-lasting immunity by generating high-affinity antibodies upon antigen re-encounter. These cells arise during primary antigen exposure and often undergo somatic hypermutation and affinity maturation in germinal centers, which enhances their ability to produce potent antibody responses [3]. MBCs rapidly differentiate into antibody-secreting plasma cells, enabling efficient and robust secondary responses [4]. Given their pivotal role in sustaining immune protection and their significant diversity [5], particularly against rapidly evolving pathogens, monitoring and analyzing the MBC repertoire has become a priority. This is particularly true for identifying monoclonal antibodies with therapeutic potential.

Single-cell high-throughput repertoire sequencing techniques have revolutionized the study of antibody responses, enabling detailed analyses of clonal evolution, somatic hypermutation, and lineage dynamics [6]. These advancements have substantially enhanced our understanding of how diverse and effective antibody responses are generated and maintained. However, these powerful techniques are limited by their inability to simultaneously determine antigen-binding specificities alongside immunoglobulin variable gene (VDJ/VJ) sequencies. Identifying antigen specificity often requires the cloning and expression of VDJ/VJ genes in cell lines to produce monoclonal antibodies (MAbs) [7]. This process is labor-intensive and time-consuming, and frequently involves the production and testing of hundreds of MAbs to pinpoint the desired antibody. For researchers in low-resource settings, these limitations are compounded by financial and technical barriers, which hinder access to methodologies that enable studies of locally relevant pathogens.

Highly efficient *in vitro* culture methods of human B cells have been previously described [8]. This protocol requires co-cultures with peripheral blood mononuclear cells (PBMCs) from the same individual to act as feeder cells to support B cell growth. Although this approach allows the estimation of antigen-specific clonal frequencies and the study of the cross-reactivity of humoral response at the clonal level, it can become often impractical due to limited sample

availability. Additionally, while these cultures efficiently stimulate clonal expansion, they do not allow for isolating unique VH/VL sequencing due to mRNA contamination from endogenous B cells in the PBMCs used as feeder cells; as such, they are not suitable for monoclonal antibody isolation. Feeder cell lines expressing activating B cell factors have emerged as an efficient alternative for isolating monoclonal antibodies from MBC and GC B cells in mouse experimental models [9, 10]. Here, we extend this approach to human B cell cultures thereby circumventing the limitations posed by the usage autologous PMBCs as feeder cells. To the best of our knowledge, this is the first description of a highly efficient and low-cost approach for simultaneously identification of antigen specific human B cell clonotypes, their V-region sequencing and production of mAbs.

We present an efficient, integrated, and low-cost human B cell culture method for studying the repertoire of human MBCs and isolating potentially neutralizing monoclonal antibodies of clinical interest. Lessons learned from the COVID-19 pandemic have alerted for the importance of empowering researchers in low-resource settings with the necessary tools and methodologies to address diseases that disproportionately affect low-income regions. The low-cost method described here for the isolation and production of mAbs of interest not only fosters scientific advancement but also builds local research capacity and drives innovation tailored to specific health challenges. Furthermore, it promotes global health equity by ensuring that all regions benefit from scientific progress and improved healthcare outcomes.

To illustrate the power of the method described here, we use samples from SARS-CoV-2 convalescent patients and vaccinated donors to perform a comprehensive analysis of the MBC repertoires specific to the Spike-protein of SARS-CoV-2 and its variants of concern (VOCs). This approach enabled unbiased and highly sensitive detection of antigen-specific human MBCs, demonstrating significant advancements in several critical areas of monoclonal antibody discovery: (i) epitope-specific studies distinguishing between S-protein RBD, NTD, and S2 regions, (ii) cross-reactivity studies across SARS-CoV-2 VOCs, (iii) monoclonal antibody isolation from single-cell cultures suitable for neutralization assays (iv) single-cell culture lysates suitable for VDJ sequencing, showing no distortion in the antibody repertoire, and identification of several public clones. Lastly, we provide a proof of concept by sequencing and expressing V-regions of two public clones, identified using the present methodology, for functional characterization in neutralization assays. Overall, the method presented here offers a powerful tool for laboratories in low-income countries, allowing healthcare researchers to conduct critical immunological studies and develop targeted therapies in an autonomous manner.

Results

Establishing effective culture conditions for *in vitro* expansion of human memory B cell

Our group previously described an efficient method for analyzing the mouse B cell repertoire, combining high-efficiency B cell cultures with single-cell RT-PCR for Ig variable gene amplification and sequencing [10]. This approach used murine B cells cultured on a layer of S17 stromal cells [11], as feeder cells, with mitogens such as LPS, CpG, and Pam3Cys, promoting proliferation and differentiation of these cells *in vitro*. Leveraging this strategy, we designed here a similar system for human memory B cells (MBCs) by incorporating feeder cells to provide essential factors for B cell proliferation and antibody secretion.

To select the most efficient feeder cell for human B cell culture system, we tested three feeder cell lines previously described in the literature: S17, 40LB, and NB21. S17 is a mouse bone marrow stromal cell which supports myelopoiesis and B lymphopoiesis [11]. The 40LB feeder cells, derived from the 3T3 fibroblast lineage, were engineered to express CD40L and BAFF, simulating germinal center conditions [9]. NB21 cells, a derivative of 40LB, were further engineered to express IL-21, enhancing B cell survival and Ig secretion [12]. Sorted memory B cells (MBCs) from a seronegative donor for SARS-CoV-2 antibodies were cultured in limiting dilution assay (LDA) at different cell densities and the frequency of immunoglobulin-secreting cells were quantified after 7 days of culture by ELISA. The frequency of cloneable MBCs was calculated, according to the Poisson distribution, as the seeded MBC number at which 37% of cultures were negative for antibody detection (shown by the horizontal dotted line). We observed that NB21 cells significantly improved B cell cloning efficiency compared to S17 and 40LB feeder lines (**Supplementary Figures 1A, 1B**).

While murine B cells can be efficiently stimulated with LPS [10, 13], this approach was ineffective for human B cells in our hands, consistent with previous findings [8]. Pinna et al. demonstrated optimal conditions for human MBC proliferation using R848 or CpG in combination with high doses of IL-2 (1,000 U/mL). We compared R848 and CpG (both in the presence of hrIL-2) in our culture system, using NB21 as feeder cell, at concentrations of 2 µg/ml and 10nM, respectively. No significant differences in their efficacy to support memory B cell proliferation and antibody production were observed (**Supplementary Figure 1C**). Therefore, R848 was chosen for further experiments as its cost-effectiveness and its dual role as a TLR7 and TLR8 agonist [14]. Finally, given that the proposed method is designed to be applied in low-resource settings, we compared manual mechanical cell plating with automated cell plating with a robotic system integrated into the sorting device. The results demonstrated comparable frequencies of responding B cells, with a representative experiment yielding 55%

and 59% responder frequencies for robotic and manual plating, respectively (**Supplementary Figure 1D**).

Validation of a culture method for comprehensive and unbiased analysis of the human memory B cell repertoire

Our LDA culture system allows for probing a reliable percentage of responding B cells. We then applied this methodology to analyze Spike-specific MBC repertoire in SARS-CoV-2-exposed donors and convalescent patients. These experiments aimed to assess the sensitivity and potential of our system for detecting and characterizing antigen-specific B cell responses. We first evaluated antibody titers of anti-SARS-CoV-2 Spike reactivity in sera from three cohorts of individuals, pre-COVID, exposed to SARS-CoV-2 without clinical symptoms and COVID-19 convalescent patients. Not all individuals exposed to a virus necessarily contract the disease, as observed among frontline health professionals during the COVID-19 pandemic [15]. In fact, when comparing the pre-COVID serological titers with titers in individuals exposed to the virus but who tested negative for viral detection, and convalescent individuals, we observed that the exposed-negative group had significantly higher spike-specific IgG levels compared to pre-COVID samples. Convalescent patients sampled 20 to 180 days after symptom onset exhibited much higher IgG titers compared to the exposed-negative individuals (**Figure 1A**). These findings suggest some degree of antigen-specific immunity in the exposed-negative group. This prompted us to investigate whether our assay would be sensitive enough to reveal these anti-S specific B cells in the MBC repertoire of SARS-CoV-2 exposed-negative group.

To assess the frequency of responder cells, we sorted total switched memory B cells from both SARS-CoV-2 exposed-negative individuals and convalescent patients and cultured them under LDA conditions. The gating strategy used to isolate total switched memory B cells (swMBCs) $CD19^{+}CD27^{+}CD38^{-}IgD^{-}$ cells is shown in **Figure 1B.** For these initial experiments, we have not used the traditional bait strategy to sort S-specific MBCs, as illustrated in **Figure 1C**, opting to instead to explore the unbiased repertoire. The percentage of responding cells ranged from 14% to 60%, with no significant differences observed between negative and convalescent patients (**Figure 1D**). Quantification of the number of responding B cell clones per culture ensures accurate determination of the frequency of B cells reactive to a given antigen in each sample [8]. To further ensure that our method remained unbiased towards an antigen-specific responses, we adjusted cell plating densities to calculate the percentage of B cells secreting Spike-specific antibodies. Individuals who were exposed-negative showed a lower percentage of S-specific secreting MBCs, averaging 0.2%, compared to 1.6% of convalescent patients (**Figure 1E**). Interestingly, the frequency of IgG+ MBC specific to Spike

protein tend to correlate with serum IgG anti-S levels in most convalescent donors (**Figure 1F**). These findings are consistent with the serological analysis and demonstrates that the culture method has sufficient sensitivity to distinguish samples from convalescent donors and exposed-negative individuals.

While LDA cultures can efficiently quantify antigen-specific MBCs frequencies, these cells constituted a very small fraction of the entire MBC repertoire, Moreover, bulk culture LDA systems prevent mRNA isolation from individual B cell clones, which is required for downstream transcriptional analysis of the antigen-specific VH/VL repertoire. Single-cell cultures **(**SSC**)** derived from total MBCs are thus necessary to properly address the analysis of VH/VL repertoire. However, as noted above, antigen specific MBCs are a very small fraction of the entire MBC repertoire making their identification challenging. Sorting with antigen baits offers a strategy to circumvent this limitation. Therefore, we implemented single-cell cultures (SCC) of antigen-bait sorted MBCs to evaluate whether our culture strategy could successfully support the expansion of individual B cells. In the SCC experiments, S-specific MBCs were sorted using Wuhan strain Spike protein labeled with two different fluorochromes, APC and FITC, to ensure cell specificity to the antigen (**Figure 1C**). Individual cells were cultured in separate wells with NB21 feeder cells and R848 + IL-2 stimulation. After 7 days of culture, supernatants were collected and analyzed for Ig secretion and Spike-specificity by ELISA. Responder cells in SCCs matched those observed in LDAs (**Figure 1G and H**), confirming that SCCs reliably support B cell growth and differentiation. Antigen baiting enriched Spike-specific MBCs over 30-fold, increasing the proportion of antigen-specific clones from 1.6% in LDA to 50% in SCC (**Figure 1G and H**). These results demonstrate the utility of antigen-baited SCCs for isolating monoclonal antibodies, characterizing rare, antigen-specific B cell clones and enabling downstream analysis of their transcriptional profiles.

Single-cell cultures (SCCs) for antigen-directed analysis of the Ig repertoire and monoclonal antibody isolation

The SCC enables access S-specific MBCs and the antibodies secreted by individual B cells after their differentiation into antibody-secreting cells *in vitro*. To further validate the method, we selected a cohort of eight blood donors with a history of SARS-CoV-2 vaccination and/or infection who exhibited high levels of serum-specific antibodies (**Supplementary Figure 2**). Spike-specific MBCs were sorted and subjected to SCCs. After 5 to 7 days of culture, approximately 250 µL of Ig-enriched supernatant was obtained from each SCC well, providing sufficient volume to test for total Ig secretion and multiple specificities of the same antibody by ELISA. For each individual donor, the total amounts of Ig secreted by individual MBC clones in the SCC are displayed in **Figure 2A**, with the frequency of responding B cells

varying from 22% to 54%. An average of cloning efficiency of 37% across donors was observed, as measured by total Ig secretion (**Figure 2B**). Among the 592 mAbs produced by these responding MBCs, 312 exhibited IgG reactivity against the Spike protein of the Wuhan strain. The proportion of Spike-specific MBC clones varied among donors, ranging from 29% to 71% of the Ig-positive wells (**Figure 2C and Supplementary Table 1**). On average, 51% of the clones were identified as S-positive (**Figure 2D**), consistent with our findings from the SCC in **Figure 1H**.

The SARS-CoV-2 Spike protein is a trimeric structure consisting of three identical subunits, each with distinct functional regions, including the S1 and S2 subunits, as depicted in **Figure 2E**. The S1 subunit contains the receptor-binding domain (RBD), and the N-terminal domain (NTD), while the S2 subunit facilitates the fusion of the virus with the host cell membrane. The RBD is critical for viral entry, as it directly interacts with the ACE2 receptor of human cells, making RBD-specific antibodies highly neutralizing due to their ability to block this interaction [16]. NTD-binding antibodies destabilize the Spike protein trimer, impairing its function and reducing infectivity [17, 18]. To further characterize the mAbs obtained, we analyzed their binding capacity to the RBD and NTD regions by ELISA.

On average, donors exhibited higher serum IgG levels against RBD compared to NTD (**Supplementary Figure 2C**). Consistently, RBD-specific clones accounted for 33% of cellular responses, compared to 14% NTD-specific clones, aligning with previous studies. Notably, 53% of clones bound to unknown regions, outnumbered those targeting RBD or NTD (**Figure 2F and G**). We observed a bimodal distribution in the percentage of RBD-specific clones across different donors (**Figure 2G**). For example, donors 1, 2, and 3, who received the CoronaVac (CV) vaccine, had a higher proportion of clones recognizing unknown regions, as these clones were negative for both RBD and NTD specificity (**Figure 2F**). Donor 4, also vaccinated with CV, had a history of multiple infections with Wuhan and Omicron variants, contributing to a broader response. In contrast, donors 5, 6, and 7, vaccinated with AstraZeneca (AZ), exhibited a higher a frequency of RBD-specific clones. Notably, donor 8, also vaccinated with AZ, displayed a higher proportion of clones binding to unknown regions (**Figure 2F**). When donors were grouped by vaccine type, distinct patterns of clone specificity emerged. Donors primed with CV exhibited significantly fewer RBD-specific clones compared to those primed with AZ, resulting in a higher frequency of clones recognizing unknown regions (**Supplementary Figure 2D**).

Together, these results demonstrate the ability of the SCC approach to distinguish between different epitopes within the same antigen.–The observed frequencies of domain-specific clones are consistent with reports from other SARS-CoV-2-infected cohorts [19], suggesting

that the SCC method accurately represents the underlying antibody repertoire without introducing artifactual biases.

Comparative cross-reactivity analysis of SCC-derived mAbs against SARS-CoV-2 spike protein variants

During the COVID-19 pandemic, identifying monoclonal antibodies (mAbs) capable of targeting evolutionarily conserved epitopes in the SARS-CoV-2 Spike protein became a major focus due to the virus's high mutation rate. To demonstrate the analytical capacity of our platform, we conducted a cross-reactivity study using mAbs derived from SCCs obtained from donors with varying anti-Spike serum IgG levels from different variants (**Figure 3A**). Using ELISA, we tested the reactivity of these mAbs against the Spike proteins of four major variants of concern (VOCs): Beta ("B"), Delta ("D"), Gamma ("G"), and Omicron BA.2 ("O"). Across the VOCs, the mAbs exhibited a similar average frequency of immunoreactivity, ranging from 46% to 54%, except for Omicron, which showed a lower average of ~30%. The mean immunoreactivity frequencies of mAbs for each variant, stratified by donor, are illustrated in **Figure 3B**. While these data provide an overview of variant recognition by mAbs, they do not differentiate between strain-specific and cross-reactive responses.

To further dissect cross-reactivity, we analyzed 592 mAbs isolated from eight donors. Among these, 217 clones showed no binding to any Spike protein variant (R0), and 312 clones were reactive to the Wuhan strain, with 15 clones binding exclusively this strain. A total of 375 clones were categorized into five reactivity groups based on their binding profiles, encompassing 31 distinct and overlapping categories. The R1 group included clones reactive to a single strain, while R2, R3, and R4 groups represented mAbs binding to combinations of two, three, and four strains, respectively. The R5 group contained mAbs that were reactive to all five tested strains. These reactivity groups are detailed in **Figure 3C and Supplementary Table 1**, with each group assigned labels reflecting the VOCs recognized, such as "WBO" for clones reactive to the Wuhan, Beta, and Omicron variants.

We analyzed the distribution of these categories among donors, highlighting the domain-specific binding for the R5 clones, as they exhibit the most cross-reactivity among all tested VOCs (**Figure 3D**). Within the R1 group, we found 15 clones binding exclusively to Wuhan, and 12, 11, 10 and 8 mAbs binding to Gamma, Delta, Omicron and Beta, respectively. The R1 group, representing strain-specific antibodies, may serve as critical tools for immunological assays requiring high specificity. Similarly, for mAbs in the R2 and R3 groups, which bind to combinations of two or three strains, could be valuable for immunocompetition assays probing inter-variant interactions. The R4 group, comprising antibodies reactive to all but one variant, offers unique opportunities to identify molecular signatures of broad binders and to explore

structural or genetic differences responsible for reduced binding to specific VOCs, such as Omicron. Comparative analyses between R4 clones and R5 mAbs could yield insights into the molecular features that contribute to broad reactivity. Antibodies in the R5 group, which recognize all five variants, are suggestive of binding to highly conserved epitopes, making them particularly valuable for therapeutic applications.

While a distinct distribution of cross-reactive clones was observed across donors (**Figure 3D**), most clones were grouped in R4 with 111 clones, 95 specifically in the R4 (WDBG) category, and R5 with 152 clones (**Supplementary Table 1**). We performed a comparative analysis of mAbs within these two categories, particularly the R4 (WDBG) group, recognizing all strains except Omicron, and the R5 group (**Figure 3E**). Broad cross-reactive clones are typically expected to target conserved regions of the Spike protein, such as the S2 region, making RBD and NTD less likely targets. This assumption holds for R4 (WDBG) antibodies, with 82% of clones binding to the putative S2 region (non-RBD/NTD). Surprisingly, 54% of the R5 mAbs bound either RBD (35%), NTD (15%), or both (4%), suggesting these antibodies may possess substantial broadly neutralizing potential.

Although the analysis performed effectively dissects the frequency of strain-specific and cross-reactive mAbs, it did not provide insights into the affinity of antibody recognition. To address this limitation, we utilized a heatmap representation as an alternative approach to visualize the complexity of cross-reactive analysis, providing at least a semi-quantitative assessment of the binding potential of each mAb. Binding intensity was evaluated as the ratio of ELISA optical densities (O.D. Ratio), antigen-specific O.D./total Ig O.D. **Supplementary Figure 3** illustrates the binding intensity of each R5 mAb isolated to the Spike protein of the tested VoCs, including key neutralizing antibody targets such as the RBD and NTD. The clones are organized in descending order of binding intensity to Wuhan strain, numbered sequentially from R5-001 to R5-152 (**Supplementary Figure 3A)**. They are also ordered based on Omicron binding intensity (**Supplementary Figure 3B**). Notably, mAbs exhibiting higher binding intensity for Wuhan Spike are predominantly RBD-specific. This visualization facilitated the identification of binding clusters, enabling the selection of specific clones tailored to the requirements of particular study designs. For instance, in the heatmap, we highlight clones chosen for downstream functional analysis, demonstrating the utility of this approach in prioritizing candidates for further investigation.

Supernatants from single-cell cultures (SCCs) are sufficient for neutralization assays and selecting potential neutralizing candidates

To functionally characterize the broadly binding antibodies, we selected three mAbs for testing in a pseudovirus neutralization assay against the Omicron variants BA.1 and BA.2: two

RBD-binding mAbs (R5-004 and R5-038) and one mAb that does not appear to bind either RBD or NTD (R5-053). The Omicron strain was chosen due to its generally lower intensity of binding observed in prior assays and its high divergence compared to the original Wuhan strain. As shown in **Figure 3F** these mAbs exhibited varying degrees of neutralization efficacy, revealing varying degrees of neutralization efficacy against BA.1 variant. The RBD-binding mAb R5-004 demonstrated strong neutralization potential, achieving half-maximal inhibitory concentration (IC50) values in the range of 0.001–0.01 µg/mL. In contrast, RBD-binding mAb R5-038 and the presumed S2-binder R5-053 showed moderate to negligible neutralizing activity, with IC50 values ranging from 0.01–0.1 µg/mL for the first and a limit of 50% neutralization at the highest concentration used (> 0.1 µg/mL), respectively. Notably, none of the tested mAbs were able to neutralize the BA.2 variant (data not shown), underscoring the increased challenge posed by this more divergent Omicron subvariant. The systematic evaluation of SCC-derived mAbs underscores the utility of our platform in mapping cross-reactive and strain-specific antibody responses. These findings lay the groundwork for developing diagnostic and therapeutic tools targeting SARS-CoV-2 and its evolving variants.

SCC method enables study of immunoglobulin repertoire and reveals convergent V region rearrangements

A limitation of previous B cell culture systems is the reliance on autologous PBMCs as feeder cells [8], which hinders the isolation of pure mRNA products from memory B cells (MBCs) expanded *in vitro* due to contamination from endogenous PBMC-derived B cells. To address this, we evaluated the suitability of the SCC methodology for studying the immunoglobulin repertoire at the transcriptional level. Ex-vivo expanded SSC MBCs mRNAs were subjected to Ig heavy and light chain sequencing using V region-specific RT-PCR followed by Sanger sequencing.

We sequenced a total of 240 of Ig-secreting MBCs, of which 220 were identified as IgG+ Spike-specific clones. To validate that our culture system did not distort the B cell repertoire, we analyzed the V_H gene segment usage and compared the frequencies to a dataset of healthy individuals, and previous COVID-19 studies (**Figure 4A**). Our findings revealed that gene segments IGHV3-30, IGHV5-51, IGHV3-66, and IGHV1-24 were significantly overrepresented in our cohort, whereas IGHV1-18, IGHV3-23, and IGHV1-69 were underrepresented (**Figure 4A**). Notably, the high frequency of IGHV3-30 aligns with its consistent identification in SARS-CoV-2 antibody repertoire studies [20-24].

Throughout the COVID-19 pandemic, significant efforts were made to identify common features of protective antibody responses against SARS-CoV-2 [21, 25, 26]. A seminal study highlighted specific patterns in the immunoglobulin V region, such as V gene usage bias and

CDR-H3 composition, associated with binding to RBD, NTD, or S2 regions [23]. Here, we compared our data to these previously described patterns to identify convergent antibody responses. Each clone had their mAb-enriched supernatants tested for binding to the full Spike protein and to isolated RBD and NTD domains. This allowed classification of the clones into three groups: RBD+ (S1), NTD+ (S1), and non-RBD/NTD (putative S2). Among 220 S-binding clones, 25% were RBD+, 13% were NTD+, and 62% were RBD-/NTD- (putative S2-binding clones, **Figure 4B**).

Efforts to identify potent neutralizing antibodies against SARS-CoV-2 have highlighted the importance of paralogous genes IGHV3-66/V3-53, which are enriched in RBD-binding clones [27-32]. In our data, IGHV3-66 was five times more frequent compared to the healthy repertoire (**Figure 4A**). Although only 25% of total clones were RBD+ (**Figure 4B**), 71% of IGHV3-66 clones were RBD+ (**Figure 4C, 4D**). Conversely, a strong bias toward IGHV3-30 usage has been observed in S2-binding antibodies [23]. Consistent with this, most IGHV3-30 clones in our study were classified as RBD-/NTD- (**Figure 4C, 4D**). Light chain V gene usage also exhibited domain-related biases. For instance, IGKV3-20 was associated with S2-targeting antibodies, while IGKV1-9 and IGKV1-33 were prevalent among RBD-binding clones (**Supplementary Figure 4A and 5A**) [30].

Since our mAbs were tested for RBD and NTD binding via ELISA but not for S2 binding, we cannot experimentally confirm that the putative S2 clones specifically target this region. To address this limitation, we performed *in silico* docking studies to better assess our presumption. First, we validated the docking approach by submitting two RBD-binding clones for analysis, which confirmed their preferential binding to the RBD region of the Spike protein (**Supplementary Figure 4A**). To investigate whether the putative S2-binding clones indeed targeted the S2 region, we selected four RBD-/NTD- clones for docking analysis, including two encoded by the IGHV3-30 gene segment (22E1P2E08 and 22E1P1B05). The docking results supported their binding preferences for regions within the S2 domain (**Supplementary Figure 4B**), providing further evidence for their classification as S2-binding clones.

We next investigated whether we could identify convergent paired IgH/IgL antibody sequences in our dataset that aligned with sequences reported in other SARS-CoV-2 studies. Convergent sequences were defined as those sharing the same VH/JH and VL/JL gene usage (allowing minor exceptions for light chains) and exhibiting at least 80% CDRH3 sequence identity. Despite the substantial combinatorial and junctional diversity of the human antibody repertoire, we identified at least 10 clones from our dataset that matched sequences reported in independent SARS-CoV-2 studies. Our analysis revealed four RBD-specific sequences and six putative S2-specific sequences highly similar to clones described in prior datasets (**Figure**

4E), providing further validation of our methodology and supporting the conserved nature of these antibody responses.

The distribution of CDR-H3 amino acid length reflected a typical human repertoire [33], with 14 amino acids being most frequent in RBD-/NTD- clones and 11 amino acids predominant in the RBD+/NTD+ group (**Supplementary Figure 5B and C**). This aligns with findings from Wang et al., where three major S2-binding clusters had CDR-H3 lengths of 14 amino acids [23]. Interestingly, the mean CDR-H3 length for NTD-binding clones was longer at 18 amino acids compared to 15 for RBD and RBD-/NTD- clones (**Supplementary Figure 5C**).

Charge distribution within the CDR-H3 loop was similar across groups, with a tendency toward neutrality (**Supplementary Figure 5D and E**). Overall, there was no difference in amino acid content between RBD-/NTD- (S2) and RBD+/NTD+ (S1) groups (**Supplementary Figure 4F**). To delve deeper into potential domain-specific differences, we analyzed clones with biased CDR-H3 lengths—14 amino acids for the RBD-/NTD- group and 11 amino acids for the RBD+ group—for amino acid composition. Significant differences were observed: RBD-/NTD- (S2) clones with 14 amino acid CDR-H3 loops showed increased use of neutral amino acids such as Tyr, Gly, and Ser, compared to RBD+ clones (**Supplementary Figure 5G and data not shown**). A conserved motif 97[S/G]G[S/N]Y100 was identified in RBD-/NTD- clones such as 22E1P1B05 (**Figure 4E and Supplementary Figure 4B**), consistent with previous studies [23]. In contrast, clones with 11 amino acid loops showed no preference for neutral amino acids in either S1 or S2-targeting groups (**Supplementary Figure 5G**).

The level of somatic hypermutations (SHM) did not seem to differ among clones that target the different domains (**Figure 4F**). The 240 clones were also analyzed regarding the antigenic breadth, being classified by its ability to recognize S protein by cross-reactivity level, R0-R5 (**Figure 4G**). Importantly, the largest group was R5 (41.7%) followed by R4 (32.5%). The main difference between R5 and R4 is the ability to recognize Omicron's S protein, which is the most distinct S protein tested. Clones that recognize the 5 VOCs' including Omicron (R5) seem to accumulate point mutations in comparison to those that cannot bind Omicron (**Figure 4H**). This suggests a role for SMH and affinity maturation to improve antibody breadth by cross reactivity.

Together, these findings establish the SCC platform as a powerful and reliable tool for comprehensive immunoglobulin repertoire studies, while highlighting critical conserved features of SARS-CoV-2 convergent antibody responses.

SCCs enable antigen-specific and functional mAb screening, saving time and resources before scale-up production

While the SCC methodology demonstrated robustness in antigen-specific and cross-reactivity analyses, a key limitation lies in the quantity of antibodies produced, which is

sufficient only for the initial screening assays. However, since single B cell clones' VH/VL sequences can also be retrieved through this approach, the methodology enables the use of this sequence information for medium to large-scale production in transfected cell lines. We selected two mAb clones retrieved from MBCs for medium/large-scale production. These clones represent promising candidates for downstream applications, including functional assays, structural studies, and therapeutic development.

Two public clones, identified as RBD-binders through our screening assay, were selected for cloning and expression in HEK293 cells. These clones were encoded by VH3-53 (LBL01) and VH3-66 (LBL02), both using VK1-9 for their light chains. The CDR-H3 and CDR-L3 sequences, along with V and J segment usages, are shown in **Figure 5A**. Computational docking analysis confirmed that both clones bind to the RBD (**Figure 5B**). Further blind docking analyses against several VOCs revealed limited cross-reactivity for LBL01, whereas LBL02 displayed the potential to a broader specificity as distinct docking runs converged to a similar binding site (**Figure 5C**). Accordingly, molecular dynamics simulations of the refined interaction poses followed by binding free energy calculations (ΔG_{bind}) showed a stronger interaction of LBL02 to RBD (-49.2 kcal/mol), as opposed to LBL01 (-42.3 kcal/mol), suggesting that LBL02 may be better suited to resist viral escape due to a more stable binding interface.

We tested the medium-scale production of these two mAbs in binding assays against the following VOCs: Wuhan, Delta, Beta, Gamma, Omicron (BA.2), as well as the isolated RBD and NTD domains (**Figure 5D**). Both antibodies were confirmed to target the RBD site. Titration experiments demonstrated that LBL01 exhibited relatively weak binding to the S-protein from VOCs compared to LBL02, which displayed strong apparent affinity to all VOCs tested. To assess the neutralization capacity of these mAbs, we performed pseudovirus neutralization assays against the Wuhan strain and VOCs, including Delta, Beta, Gamma, and Omicron (BA.2, BA.1, and XBB). Consistent with binding and *in silico* analyses, LBL01 showed weaker neutralization against Delta, Ba.1 and Wuhan strains, but still retained some neutralization capacity against the more recent Omicron subvariants BQ.1 and XBB, albeit limited. While LBL02 exhibited robust neutralization against Delta and Wuhan strains that decreased sharply against Omicron subvariants. (**Figure 5E**).

Altogether, these findings demonstrate that our SCC screening technique is efficient for identifying and selecting clones with the desired specificity and potential neutralizing capacity before scaling up production. This method saves time and resources typically required for traditional cloning and expression workflows, providing a streamlined approach for monoclonal antibody discovery.

Discussion

Memory B cells are essential components of the adaptive immunity, providing rapid and robust responses upon re-exposure to pathogens. By isolating and characterizing these cells, researchers can explore the mechanisms underlying long-term immunity, yielding valuable insights for the development of vaccines and immunotherapies. Such studies are particularly crucial for addressing emerging infectious diseases, where timely and precise immune responses can be pivotal in controlling outbreaks. Research on MBCs has already revolutionized treatments for diseases like COVID-19, with monoclonal antibodies being deployed as effective therapeutic agents. These studies not only deepen our understanding of immunity but also provide practical tools for combating infectious and autoimmune diseases [34-36]. Our group has developed an efficient method for studying the mouse B cell repertoire, combining high-efficiency B cell cultures with single-cell RT-PCR for Ig variable gene amplification and sequencing [10]. This approach provides access to the entire naïve B cell repertoire by cultivating nonspecific cells for subsequent specificity analysis, which is crucial for understanding immune responses to pathogens and advancing vaccine development. While antibody titers in serum provide a snapshot of circulating immunity, MBCs represent the capacity for rapid and robust secondary responses upon antigen re-exposure, offering a more dynamic view of immune memory. Here, we adapted this methodology to analyze the human MBC repertoire and established a streamlined pipeline for isolating specific monoclonal antibodies. This initiative aims to make the process accessible to researchers in low-income countries, empowering them to address local infectious disease challenges with innovative solutions.

We began by optimizing the culture conditions for human MBCs. Through comparative analysis of different feeder cell lines, we found that NB21 cells, engineered to express IL-21, as the most effective in supporting MBC survival and promoting immunoglobulin secretion. IL-21 likely boosts immunoglobulin production, particularly IgG, which is crucial for analyzing the antigen-specific antibody repertoire in MBCs. Additionally, IL-21 can synergize with other cytokines, such as IL-2 or IL-4, to optimize B cell proliferation [37]. This finding underscores the importance of selecting the appropriate feeder cells to improve *in vitro* models for studying human immune responses and monoclonal antibody production. It is noteworthy that all the feeder cells used in our study were derived from mice, yet they effectively support the growth and differentiation of human B cells in culture. This cross-species compatibility suggests that key survival and activation signals provided by these feeder cells may be conserved across species.

In our culture system, we incorporated polyclonal stimulation for B cells, drawing inspiration by Pinna et al. (2009), who demonstrated that human MBCs can be cultured with TLR agonists

to analyze antibody responses during viral infections. TLR stimulation mimics natural infection signals, offering a model to study immune responses and identify therapeutic targets. Pinna et al. optimized MBC proliferation using R848 or CpG combined with high-dose IL-2 (1,000 U/mL) [8]. Given R848's cost-effectiveness and dual activation of TLR7 and TLR8, we chose R848. Additionally, we compared manual cell plating with automated robotic plating integrated into the sorting device. While robotic systems save time, they are costly and less accessible in low-income settings. Manual plating, on the other hand, offers precise control of cell concentrations, and allows real-time adjustments based on experimental needs. Variability in MBC counts among donors, influenced by genetic diversity, adds complexity yield estimation. For these reasons, we opted for manual plating to better control the cell density and ensure consistency across experiments.

Having established a functional method capable of culturing MBCs with a reliable percentage of responding cells, we showed that the methodology is sensitive enough to detect and characterize both total and antigen-specific responses in SARS-CoV2-exposed donor and convalescent patients. Notably, during 2020, vaccines for COVID-19 were not yet available, and the exposed donors in this study were frontline health professionals during the pandemic. While not all exposed individuals that were exposed to a virus necessarily contract the disease, we confirmed that these donors possessed some degree of antigen-specific immunity in their serum. This observation prompted us to investigate whether such immunity could be detected within the MBC repertoire using our limiting dilution assay (LDA) culture system. To achieve this, we focused on sorting IgD- MBC. IgD is a B cell receptor isotype predominantly found on the surface of naïve, antigen-inexperienced B cells. Therefore, the absence of IgD indicate that the B cell has been activated and has probably undergone class-switch recombination, a hallmark of memory B cells, and most likely a IgG secreter [38]. The frequency of responding cells was calculated using the Poisson distribution, which models the number of events occurring in a fixed interval under the assumption of independence and constant average rate. Our analysis revealed an average response of 40% of responding cells, with no difference between the two groups (exposed and convalescent patients). This response rate aligns with the findings of Pinna et al. (2009), who observed a similar frequency using LDA cultures on peripheral blood mononuclear cells (PBMCs) as feeder cells. These results underscore the sensitivity and reliability of the proposed methodology for studying MBC responses in diverse donor populations.

Beyond measuring total responding cell frequency, the ability to detect low-frequency antigen-specific MBCs is crucial for understanding immune memory, given the vast antigenic repertoire that MBCs must encode over a lifetime. Traditional approaches often struggle to characterize these rare populations due to their low abundance. Following Pinna et al 2009,

here we analyzed the antigen-specific repertoire using limiting dilution assay (LDA) cultures, performing ELISA against the Spike protein with supernatant collected from wells with high cell density, where specific B cells are more likely to be found. Our methodology demonstrated sufficient sensitivity to distinguish SARS-CoV-2-exposed donors from convalescent patients sampled in 2020. Importantly, the correlation observed between Spike-specific MBC frequencies and serum anti-Spike IgG levels further validates the sensitivity and relevance of this method. Similar correlations have been reported in previous studies of patients exposed to antigens through immunization or infection [5], reinforcing the robustness of this method. The supernatants collected from the LDA can be repurposed to access the frequency of responses to unrelated antigens or immunization-derived antigens, depending on the research objective. These supernatants offer a comprehensive snapshot of one individual's immune history, containing antibodies that reflect a wide range of past exposures and immunological experiences. By analyzing these samples, researchers can identify and quantify responses to diverse antigens, yielding valuable insights into the breadth and specificity of the memory B cell repertoire.

To isolate antigen-specific cells for monoclonal antibody (mAb) production, we employed a baiting strategy using the Spike protein from the Wuhan strain conjugated to two different fluorescent markers. We show that single-cell culture (SCC) systems yield percentages of responding B cells comparable to those obtained through limiting dilution assays (LDA), while significantly enhancing the isolation of antigen-specific mAbs. Specifically, the baiting strategy increased the yield of antigen-specific mAbs by 50-fold compared to cultures without baits. By focusing on Spike-specific mAbs from a cohort of vaccinated and/or infected donors, this methodology proved effective in uncovering the specificity and functional diversity of antibodies. Moreover, it facilitated efficient analysis of antibody cross-reactivity and epitope targeting, critical for understanding immune protection against viral variants.

A key advantage of SSC approach is the ability to rapidly interrogate multiple specificities within a single antibody sample. Despite the limited supernatant volume collected from SCCs, we demonstrated the feasibility of performing pseudo neutralization and multiple ELISA assays to identify antigen-specific responses and prioritize the most promising mAbs to sequencing. This is particularly beneficial in scenarios where logistical or financial constraints prevent the sequencing of a large number of mAbs. Compared to traditional hybridoma techniques, SCCs offer a significant practical advantage by streamlining the process and eliminating labor-intensive steps such as cloning and transfection. Importantly, our data demonstrate that antigen-baited B cells maintain viability and are not prone to cell death induced by B-cell receptor (BCR) cross-linking. This highlights the efficacy of the bait strategy in substantially increasing the yield of isolated antigen-specific MBCs while preserving their functionality at the

single-cell level. These findings highlight the robustness of the SCC-based platform, emphasizing its utility for studying the antibody repertoire and advancing monoclonal antibody discovery in a time-efficient and cost-effective manner.

The method described here enabled the rapid isolation of 592 mAbs, 312 of which demonstrating reactivity to the Wuhan strain Spike protein, underscoring its capability to efficiently detect and quantify antigen-specific mAbs, while also revealing donor-to-donor variability. However, the frequency of Spike-specific MBCs was lower than expected compared to other studies employing bait strategies for monoclonal antibody isolation [20, 21]. Several factors should be considered when interpretating our findings. First, the use of an IgG-specific secondary antibody in the antigen-specific ELISA likely skewed the detection of Spike-specific MBCs towards IgG+ subsets, potentially underestimating contributions from IgM+ or IgA+ MBCs. This limitation is particularly relevant given the diverse roles of IgM and IgA in early and mucosal immune responses, respectively [39, 40]. To address this, ongoing studies in our lab aim to profile the isotype diversity in circulating B cells to provide a more comprehensive view of antigen-specific MBCs (data not shown). Additionally, we observed that some Spike-specific sorted MBCs may not produce detectable antibodies in the antigen-specific ELISA due to low binding affinity or insufficient secretion, which could explain the lower-than-expected frequencies. These limitations underscore the importance of refining detection methods to capture a broader spectrum of MBC responses. Expanding the adaptation of this approach to other viral antigens or disease contexts warrants investigation. By adapting the bait strategy to target different antigens, this platform could become a versatile tool for studying MBC responses in various infectious diseases, including emerging pathogens. Its cost-effectiveness and scalability also make it particularly appealing for application in resource-limited settings, where access to advanced technologies may be constrained. This methodology not only broadens the scope of immune response studies but also offers a practical and equitable solution for addressing global health challenges.

Given the well-known immunodominance of the receptor-binding domain (RBD) and N-terminal domain (NTD) of the Spike protein [41, 42], we stratified mAb specificities to these regions. The RBD is well-established as a critical target for neutralizing antibodies due to its role in ACE2 receptor binding, a key step in viral entry [41]. However, the RBD is under high mutational pressure, particularly in variants of concern (VoCs) like Delta and Omicron, presents a significant challenge for vaccine-induced and natural immunity. Antibodies binding to evolutionary conserved epitope within RBD that can recognize all VoCs hold great potential for preventing infections across diverse strains. Similarly, the NTD plays a multifaceted role in viral attachment and entry but is also prone to mutations and deletions that alter antigenicity and enable immune evasion [42]. These structural changes in both RBD and NTD contribute

to the virus's ability to escape recognition, complicating vaccine efficacy and the design of therapeutic antibody. Interestingly, the majority of isolated mAbs in this study were non-RBD/NTD specific, suggesting these antibodies may target conserved regions such as the S2 subunit of the Spike protein. The S2 region, which mediates viral fusion, is less prone to mutations compared to S1, making it an attractive target for broad-spectrum neutralizing antibodies. While RBD- and NTD-specific antibodies accounted for significant proportions of our isolates, the predominance of non-RBD/NTD antibodies aligns with the literature [19]. This highlights the diversity of immune responses and the potential for non-classical epitopes to contribute to immune protection. These findings emphasize the importance of expanding the scope of epitope targeting to include conserved regions for the development of universal vaccines and therapeutics against SARS-CoV-2 and its variants.

The N-terminal domain (NTD) of the SARS-CoV-2 Spike protein is susceptible to frequent mutations and deletions, which can enable the virus to evade recognition by pre-existing antibodies. These structural changes are commonly observed in several variants of concern (VoCs), including Delta and Omicron, and significantly contribute to immune escape, thereby impacting vaccine efficacy and natural immunity. The S1 subunit of the Spike protein is the most immunodominant region of the virus, with anti-receptor-binding domain (RBD) antibodies accounting for nearly 90% of the neutralizing antibodies found in convalescent plasma from COVID-19 patients. However, the NTD of the S1 subunit also contains an antigenic “supersite” that serves as a major target for antibody responses. Notably, as SARS-CoV-2 has evolved, the S1-NTD has accumulated numerous mutations—particularly deletions—which can modify antigenicity or eliminate key epitopes. These alterations enhance the virus's ability to evade immune detection, further complicating efforts to maintain effective immunity through vaccination or natural infection [42-45]. Here we utilized the NTD protein from the Wuhan strain in the ELISA assays, given that it is a highly mutated site. As expected, our analysis revealed that, on average, the NTD region was less frequently recognized by the isolated monoclonal antibodies compared to the RBD and other unidentified regions. This finding highlights the influence of mutations in the NTD on antibody recognition and binding.

The bimodal distribution of RBD-specific clone percentages among donors became evident when grouped by vaccine type. Most recipients of the CV vaccine displayed a higher proportion of clones recognizing unknown regions, whereas 3 out of 4 AZ vaccine recipients exhibited a greater frequency of RBD-specific clones. This variation likely reflects differences in vaccination regimens, prior exposure to diverse viral variants, or underlying genetic heterogeneity among donors.

The cross-reactivity analysis revealed distinct patterns of strain-specific and broadly reactive antibodies, offering valuable insights into the immunological landscape of SARS-CoV-

2 and its variants. Importantly, the identification of R5 mAbs that bind to all tested variants highlights their utility in targeting conserved epitopes. Throughout the COVID-19 pandemic, a key priority has been the identification of mAbs, that can target conserved regions of the SARS-CoV-2 Spike protein. This is critical because the virus's high mutational rate has led to the emergence of variants with increased transmissibility or immune escape potential. Antibodies binding to conserved sites are essential for developing treatments and vaccines across multiple strains. Targeting these regions enhances the prospects for broader and more durable immunity, offering a critical advantage in controlling outbreaks and mitigating the risk posed by future variants. Strain-specific antibodies, such as those in the R1 group, also hold significant value as precise tools for detecting individual variants, making them critical for variant-specific diagnostic assays. Comparative analyses between R4 and R5 clones could provide valuable insights into the molecular features driving broad reactivity. Antibodies in the R5 group, capable of recognizing all five tested variants, likely target highly conserved epitopes. These conserved binding sites suggest a potential for enhanced neutralization breadth, making R5 mAbs particularly promising candidates. Furthermore, the ability to map binding intensities through heatmap visualizations provides a semi-quantitative framework for selecting high-affinity antibodies for clinical applications, enabling targeted vaccine design and therapeutic optimization. Additionally, the functional characterization of RBD- and NTD-binding mAbs through neutralization assays emphasizes their relevance in combating highly divergent variants like Omicron. High-efficacy clones, including R5-004 and R5-053, demonstrate the platform's capacity to identify potent neutralizers capable of maintaining activity even when standard assays indicate reduced binding. Collectively these findings highlight the platform's potential in advancing therapeutic and diagnostic applications while deepening our understanding of immune protection against SARS-CoV-2 variants.

One of the primary objectives in B cell repertoire studies is the identification of variable genes to characterize the molecular signatures of protective antibodies and to pinpoint specific VH/VL pairs for downstream expression and large-scale production of monoclonal antibodies. To achieve this, it is essential to preserve and isolate mRNA from single B cells in culture systems. Unlike the whole PBMC culture system demonstrated by Pinna et al., where PBMCs act as feeder cells, our culture system eliminates the issue of feeder cell contamination. This key improvement addresses a significant limitation of the previous method, as the presence of endogenous PBMC-derived B cells can interfere with the isolation of pure mRNA from the target MBC expanded in vitro. By removing this source of contamination, our approach enhances the accuracy and reliability of downstream analyses, facilitating more precise studies of MBC responses and monoclonal antibody discovery and production.

SCCs enable unbiased profiling of memory B cells (MBCs), uncovering convergent rearrangements in immunoglobulin variable (V) regions that align with findings from previous SARS-CoV-2 studies [21, 23, 46]. Key insights include the representation of VH gene segments, particularly IGHV3-30 and IGHV3-53/IGHV3-66, and their association with distinct Spike regions. Consistent with earlier studies, IGHV3-53/IGHV3-66 was strongly linked to RBD-binding antibodies, while IGHV3-30 was primarily associated with putative S2-targeting clones [23]. Computational docking confirmed these classifications, providing evidence for conserved binding motifs and structural preferences. The paralogous genes IGHV3-53 and IGHV3-66 are frequently described as encoding public clones across diverse populations [32, 47]. Interestingly, while most global studies report a higher prevalence of IGHV3-53 compared to IGHV3-66, our data showed a 4-fold higher frequency of IGHV3-66 among RBD-binding antibodies. This unique finding might reflect a characteristic feature of the B cell repertoire in Brazil, as a similar preference for IGHV3-66 was observed in another study involving Brazilian blood donors [20].

As a proof of concept for the method's capability to rapidly screen monoclonal antibodies (mAbs) with potential for virus neutralization and subsequent production at medium or large scale, we successfully cloned and expressed two public clones identified using the present methodology. The identification of RBD-specific clones with broad neutralizing potential, such as LBL 01 and LBL02, underscores the platform's utility in prioritizing antibodies for therapeutic and diagnostic applications. Importantly, VH/VL analysis of SCC-derived clones exhibited somatic hypermutations correlating with cross-reactivity, particularly for challenging variants like Omicron. This finding highlights the critical role of affinity maturation in generating broadly reactive antibody responses.

The presented methodology enables the low-cost screening of specific monoclonal antibodies relevant to the study by providing critical insights into binding properties, site-specificity, cross-reactivity, and functional characteristics, using the collected supernatant. An important limitation of this approach is the low volume of supernatant collected at the end of the culture period. However, this challenge can be mitigated through medium-scale antibody production targeted to the specific research question. This strategy ensures efficient use of resources by enabling the selection of cells based on prior specificity and functional testing, thereby minimizing waste. Importantly, we demonstrated that mAbs produced at a medium scale from sequenced antibodies successfully replicated the results obtained from the supernatant, reinforcing the efficacy and reproducibility of the methodology, exhibiting binding patterns consistent with those observed in ELISA assays and docking analyses.

In summary, the methodology described in this study offers a reliable, fast, and scalable approach for the isolation of mAbs with potential clinical relevance. Its cost-effectiveness and

adaptability make it particularly well-suited for laboratories in resource-limited settings, empowering researchers in low-income countries to conduct critical immunological studies and develop targeted therapies independently. Beyond facilitating therapeutic mAb discovery, this approach enhances our understanding of conserved immunological features, providing valuable insights into combating emerging SARS-CoV-2 variants and similar pathogens. By broadening the scope of immune response studies and addressing global health challenges equitably, this methodology represents a significant step toward advancing vaccine and therapeutic development worldwide.

Methods

Ethic Statement

This study was approved by the National Ethics Committee (CONEP, Brazil; CAAE: 30161620.0.0000.5257) and the local ethics committee of Fundação Oswaldo Cruz (CAAE: 3048.7120.2.0000.0008). Blood collection from the volunteers in this study was carried out at the Diagnostic Center of Núcleo de Enfrentamento e Estudos de Doenças Infecciosas Emergentes e Reemergentes (NEEDIER) located at the Universidade Federal do Rio de Janeiro and at Fundação Oswaldo Cruz, in adherence to the approved protocols

Study Participants

For this study, we enrolled fourteen patients from Brazil, collecting whole blood samples at NEEDIER to perform Limiting Dilution Assay experiments. Participants were categorized into two cohorts: Cohort 1: healthcare workers with negative PCR results (negative exposure group) and Cohort 2: convalescent individuals ranging from 20 to 180 days after their first negative PCR result. Additionally, we received 23 pre-COVID plasma samples collected at the State Hematology Institute Hemorio followed a protocol approved by the local ethics committee (CEP Hemorio; approval #4008095). We also use a Cohort 3 for monoclonal antibody isolation that consists in eight vaccinated and convalescent patients as described in Supplementary Figure 2 A. These patients were enrolled through Fundação Oswaldo Cruz, with whole blood samples collected for further analysis.

Blood sample processing

All blood samples were collected in tubes with heparin as an anticoagulant and sent to the Laboratory of Lymphocyte Biology (LBL) for subsequent PBMC isolation. To obtain the desired cell population, we followed the purification protocol using Ficoll Histopaque®-1077 (SIGMA-Aldrich cat.10771). After allowing the sample to settle for 40 minutes at RT, the tubes containing the sample were centrifuged at 1500 rpm for 5 minutes at 24ºC. Next, the plasma was removed and frozen, and the blood was carefully transferred to a 15 mL falcon tube containing 5 mL of Ficoll at a 2:1 dilution. This tube was centrifuged again, this time for 30 minutes at 400g, 24ºC, without brake or acceleration. The PBMC layer was then collected, washed with 1x PBS, and centrifuged at 1300 rpm for 5 minutes at 24ºC. After this step, the pellet was resuspended in 2 mL of ACK Lysing Buffer® (GIBCO ref: A10492-01) to lyse red blood cells, keeping the sample in the refrigerator for 5 minutes. After a wash step as described previously the cells was resuspended in FACS Buffer containing the labeled antibodies for staining.

ELISA for detection of serum immunoglobulins

For quantitative analysis of anti-SARS-CoV-2 spike protein IgG antibodies, we performed the S-UFRJ test, as described previously [48]. Briefly, high binding ELISA plates were coated with 50 µL of SARS-CoV-2 spike protein (4 µg/mL in PBS) and incubated overnight. The coating solution was removed and 100 µL of PBS 1% BSA (blocking solution) was added and the plate was incubated at room temperature (RT) for 1-2 hours. The blocking solution was removed and 50 µL of diluted 1:40 (PBS 1% BSA) patient sera were added, subsequently, the sera were serially three-fold diluted in the plate, which was incubated at RT for 2 hours. Then, the plate was washed with 150 µL of PBS (5x) and 50 µL of 1:10000 goat anti-human IgG (Fc)-horseradish peroxidase antibody (Sourthen Biotech, Birmingham, USA) were added, and the plate was incubated for 1.5 hours at RT. The plate was washed again with 150 µL of PBS (5x) and then treated with TMB (3,3',5,5-tetramethylbenzidine) (Scienco, Brazil) until the reaction was stopped with 50 µL of HCl 1N. The optical density (OD) was read at 450 nm with 655 nm background compensation in a microplate reader (Bio-Rad Laboratories, Inc, California, USA). Relative antibody levels were determined based on a cut-off (C.O) value calculated as the mean absorbance of the negative controls plus one standard deviation on the same ELISA plate. Samples with absorbance values below the C.O were classified as negative, while those with values at least two times above the C.O were considered positive.

Feeder cell lines preparation

The feeder cells are cultured in T175 flasks (Falcon, Ref #353112) until they reach confluence, using RPMI (Gibco, Ref #) supplemented with 1% pyruvate (Gibco, Ref #), 1% glutamine (Gibco, Ref #), 1% penicillin-streptomycin (Gibco, Ref #), 1% HEPES (Gibco, Ref #), 50 nM beta-mercaptoethanol (Gibco, Ref #), and 10% fetal bovine serum (FBS, Gibco, Ref #). The cells are passaged every three days. Upon reaching confluence, the cells are detached by treating them with trypsin (Gibco, Ref #) for 5 minutes at 37°C and 5% CO_2. The culture medium is collected, and the cells are washed with PBS. After centrifugation at 300g for 5 minutes, the pellet is resuspended in 10 ml of RPMI. The cells are then counted using a Neubauer chamber. For plating, 3000 NB21 feeder cells are seeded per well in 100 µl of RPMI with the aforementioned supplements and allowed to grow overnight. The following day, the cells are irradiated with 20 Gy to halt the cell cycle. This irradiation is performed at the Laboratório de Instrumentação Nuclear (LIN), Centro de Tecnologia da UFRJ.

Cell sorting

The cells were stained in supplemented RPMI using CD19 – BV421, CD38 – Pecy5, CD27 – PE, IgD – Pecy7, DUMP(CD3/CD14/CD16) – APCcy7 and Spike-protein labeled with Alexa 488 and Alexa 647 to access the swMBC population ($CD19^+CD38^-CD27^+IgD^-$) and antigen-

specific swMBC populations ($CD19^{+}CD38^{-}CD27^{+}IgD^{-}Spike^{APC+FITC+}$). Cells were sorted using MoFlo (Dako cytomation) in 5ml tubes with supplemented RPMI.

B cell cloning cultures

Sorted cells were counted and plated using different densities of cell in LDA or 1 cell per well in SCC. In LDA, since the number of B cells were variable among the patients, we plated in the first row 500 to 2000 cells in eleven columns of a 96 well culture plate flat bottom descending in a 3 fold dilution in the first 4 rows of the plate, the for last rows were plated to tending to zero so it can be possible to calculate Poisson distribution.

We plate the 100µl with the determined number of MBC (LDA or SCC) over a monolayer of NB21 cells and supplemented with the polyclonal stimuli of IL-2 (10nM) and R848 (2µg/ml). In this comparison, R848 (Resiquimod) and IL-2 were used as polyclonal stimuli, based on previous reports demonstrating their effectiveness in human B cell cultures [8]. The cells were left to grow for 5 days, then we collect 25µl of the supernatant to perform the ELISA for detect total immunoglobulin. In the day 6, we collect another 15µl to perform the antigen-specific ELISA. We stop the culture in day 7, removing and storage the supernatant with 0.02% Azide in another 96 well plate. And the B cells were harvested with 200µl of cold PBS 1x, and transferred to a PCR plate with 10 µl of TLC + 5% betamercapto for Immunoglobulin gene sequencing.

ELISA for total immunoglobulins in LDA

High binding ELISA 96-well microplates (Corning) were coated with 50 µL per well using 1:1000 dilution of Ig unlabeled (Southern Biotech #) in PBS 1x for 4°C overnight. In the next day, plates were blocked with 200µl of blocking buffer (PBS 1x with 1% of BSA) for 1h at RT. The blocking buffer was removed, and supernatant was plated diluted two times using blocking buffer in a total volume of 50µl for 2h at RT. The plates were washed five times with 200µl per well of PBS 1x. We used an Ig conjugated with HRP as a secondary antibody using a concentration of 1:4000 dilution in blocking buffer in 50µl per well. The plates were washed as described above and developed with 50 µL of TMB (Scienco, Brazil). The reaction was stopped with 50 µL of 1 N HCl, and the optical density (O.D.) was read at 450 nm with 655 nm background compensation in a microplate reader (BioRad). Positive antibody levels were determined based on a cut-off (C.O) value calculated as the mean absorbance of the negative controls plus three standard deviation on the same ELISA plate. Supernatant with absorbance values below the C.O were classified as negative, while those with values above the C.O were considered positive.

Antigen-specific ELISA

Half-area High binding ELISA 96-well microplates (Corning) were coated with 30 µL per well using 4µg/ml of the Spike-antigen (Wuhan, Delta, Beta, Gamma and Omicron BA2), produced as previously described [48] or 1µg/ml of available RBD or 1µg/ml of NTD in PBS 1x for 4°C overnight. In the next day, plates were blocked with 150µl of blocking buffer (PBS 1x with 1% of BSA) for 1h at RT. The blocking buffer was removed, and supernatant was plated diluted two times using blocking buffer in 30µl volume for 2h at RT. The plates were washed five times with PBS 1x. We used an IgG conjugated with HRP as a secondary antibody using a concentration of 1:4000 dilution in blocking buffer in 30µl per well. The plates were washed as described above and developed with 30 µL of TMB (3,3',5,5-tetramethylbenzidine) (Scienco, Brazil). The reaction was stopped with 30 µL of 1 N HCl, and the optical density (O.D.) was read at 450 nm with 655 nm background compensation in a microplate reader (BioRad). To maximize our resources, we performed the antigen-specific ELISA assays using half-area ELISA plates, which allowed us to save the supernatant and conduct more assays. For the culture supernatants, Positive antibody levels were determined based on a cut-off (C.O) value calculated as the mean absorbance of the negative controls (NB21 culture supernatants without B cells) plus three standard deviation on the same ELISA plate. Samples with absorbance values below the C.O were classified as negative, while those with values above the C.O were considered positive.

Production of SARS-CoV-2 variant pseudo-typed viruses and pseudovirus neutralization assays

SARS-CV-2 encoding plasmids: pcDNA3.1-SARS-CoV-2-S (Wuhan) was a gift from Thomas Gallagher [49]; pcDNA3.3_CoV2_P1 (Gamma), B.1.617.2 (Delta), XBB, and BQ.1 were gifts from David Nemazee [50]; pcDNA3.1-CoV2-Omicron BA.1 spike was a gift from Ben Murrell [51]. Plasmids encoding the WT (Wuhan) SARS-CoV-2 spike, VOCs (Delta and P.1 Gamma) spikes and VOC Omicron sub-lineage spikes (Ba.1; Ba.2; XBB; BQ.1) were transfected with Lipofectamin 3000 (Thermo) in Hek-293T cells and 24 hours later infected with a VSV-G pseudo-typed ΔG-luciferase (G*ΔG-luciferase) with a multiplicity of infection of 5 for 2 h before washing the cells with 1×PBS. Transfected/infected cells were incubated with fresh DMEM with 5% FCS. The next day, transfection/infection supernatants were collected and clarified by centrifugation at 300g for 10 min before filtration through a 0.45µm filter. SARS-CoV-2 pseudotyped ΔG-luciferase viruses were titrated in Vero E6 cells and aliquots stored at −80°C.

Neutralization assays were performed by incubating pseudoviruses with serial dilutions of sera or mAbs present in the supernatants from SCC monoclonal antibodies and scored by the reduction in luciferase gene expression. In brief, Vero E6 cells were seeded in a white 96-well

plate at a concentration of 2×10^4 cells per well. Pseudoviruses were incubated the next day with serial dilutions of the test samples in triplicate for 30 min at 37°C. The mixture was added to cultured cells and incubated for an additional 24 h. The luminescence was measured by Luciferase Assay System (Promega). IC_{50} was defined as the dilution at which the relative light units were reduced by 50% compared with the virus control wells (virus + cells) after subtraction of the background in the control groups with cells only. The IC_{50} values were calculated using nonlinear regression in GraphPad Prism.

Immunoglobulin sequencing from single cell cultures

To obtain single cell lysates, at day 6-7 post SCC, MBC were harvested from co-culture 96 well plates, centrifuged and suspended in 10 µL of TCL buffer (Qiagen) containing 1% 2-mercaptoethanol [52]. Cell lysate plates were immediately frozen and kept at -80°C for mRNA preservation. RNAClean XP (Beckman Coulter) was used to purify mRNA following the manufacture's instructions. cDNA was synthesized with 25 pmol Oligo-dT primer and 50 U of Superscript III reverse transcriptase (Invitrogen) in the presence of 4 U RNAsin (Promega). Reverse transcription was carried out at 42°C for 10 min, 25°C for 10 min, 50°C for 60 min and 94°C for 5 min [7]. cDNA was stored at -20°C and variable region from heavy and light chains were amplified using 4µL cDNA and primers presented in **Supplementary Table II** [53]. PCR reaction was performed with 1.25 U/ reaction of GoTaq Flexi DNA Polymerase (Promega) in the presence of 25 pmol primers, 0.2 mM dNTPs and 2 mM $MgCl_2$, as suggested by the manufacture. Cycle conditions were adapted from a previously published study [53], consisting of: 2 min at 94°C, 4 cycles of 30 s at 94°C, 30s at 50°C and 2 min at 72°C, followed by 8 cycles of 30 s at 94°C, 30 s at 55°C and 2 min at 72°C and 28 cycles of 30 s 94°C, 30 s 60°C and 2 min at 72°C. Final extension was performed at 72°C for 10 min. Heavy and light chain PCR products were purified with ExoSAP-IT (Invitrogen) according to the manufacture's instructions and sequenced with 3.2 pmol of the reverse primer. Sanger Sequencing were performed by the PSEQDNA-UFRJ facility, Biophysics Institute, Federal University of Rio de Janeiro.

Analysis of immunoglobulin sequences

Obtained sequences were converted to fasta file and submitted to gene alignment using IMGT/HighV-QUEST tool [54], in some cases Vbase 2 [55] and IgBLAST were used for confirmation. VH, DH, JH, VK, VL, JK and JL gene segments were annotated, and the number of nucleotide mismatch mutations were calculated. The human V genes usage of the antibodies from this study were analyzed as described by Agudelo et al [20]. Briefly, the frequency distributions of human V genes in anti-SARS- CoV-2 antibodies compared to 131,284,220 IgH and IgL sequences generated by Soto et al. [56] and downloaded from cAb-Rep [57], a database of human shared BCR clonotypes available at https://cab-rep.c2b2.

columbia.edu/. The two-tailed t test with unequal variance was used to compare the frequency distributions R of human V genes of anti-SARS-CoV-2 antibodies from this study to Sequence Read Archive SRP01097039. CDR-H3 analyses were performed as previously described [58]. CDRH3 logograms were plotted using the online tool https://weblogo.berkeley.edu/logo.cgi [59]. Average hydrophobicity of CDR-H3 was calculated as previously described [60].

Antibody expression and purification

The V_H and V_L antibody sequences of LBL01 and LBL02 were ordered as gBlocks (Integrated DNA Technologies) and cloned by Gibson assembly (New England Biolabs) into a customized pcDNA 3.4 vector containing a human IgG1 Fc region. V_H and V_L plasmids were mixed at 1:2 ratio and were transfected into Expi293F cells (Thermo Fisher Scientific), which were cultured at 37 °C and 8% CO_2 for 6 days, then harvested, centrifuged 4500 x g for 20 min. Antibodies were isolated from filtered (0,22µm) supernatants using Protein G Plus Agarose (Pierce Thermo Fisher Scientific) affinity chromatography, washed with 20 column volumes of PBS, eluted with 150 mM glycine-HCl pH 2.7, and neutralized with 1 M Tris-HCl pH 8.0. The antibodies were buffer-exchanged into PBS and concentrated using Pierce™ Protein Concentrators PES 30,000 MWCO centrifugal spin columns (Thermo Fisher Scientific).

***In silico* analysis of antibody binding**

Antibodies variable domain sequences were submitted to the ABodyBuilder2 module of the ImmuneBuilder program and the resulting structural models were validated using QMEANDisCo and MolProbity [61, 62]. Epitope prediction was performefsd through blind docking assays using ClusPro antibody mode [63]. Prior the submission to ClusPro, residue charges were adjusted to pH 7.4 using PDB2PQR [64]. Spike structures from 11 VOCs were recovered from the Protein Data Bank using the IDs: 6VYB (Wuhan); 8DLI (Alpha); 8DLL (Beta); 8DLO (Gamma); 7W9E (Delta); 7XO5 (Omicron BA.1); 8XZH (BA.1.1.529); 7XOA (BA.2); 7XIY (BA.3); 7XNQ (BA.4/5); 8IOU (XBB.1). The lowest-energy complex from each docking run was recovered, and the complexes were aligned in PyMOL to check for convergent binding pose[65]. The interacting amino acids were identified and used as the active residues in an information-driven docking step with the aim of refining the antibody-antigen interface. HADDOCK2.4 was used to dock the antibody models to the Spike protein (PDB ID: 6VSB) [66, 67]. The results were assessed based on parameters such as cluster size, buried surface area, and the HADDOCK score. Moreover, binding energy was estimated using the PRODIGY webserver [68].

A final validation step applied heated Molecular Dynamics to assess the thermostability of the HADDOCK-generated complexes, distinguishing true binding poses from decoys [69]. Briefly, AmberTools19 was used to insert the complexes into a truncated octahedral box which

was solvated with SPC/E water and adjusted to 0.15 M NaCl concentration. The systems were heated to an initial temperature of 310 K and equilibrated prior to a 70 ns production run. The temperature was increased to 330, 360, and 390 K at 30, 42.5, and 55 ns, respectively. All simulation steps were conducted in Amber18, and the trajectories were analyzed in cpptraj to evaluate the interface RMSD using the cut-off of 5 Å to identify stable poses.

Statistical analysis

Statistical analyses were performed using GraphPad Prism 10.0 software. Using a statistical model based on the Poisson distribution, the percentage of negative cultures obtained in ELISA assays of LDA cultures, plotted as a function of the number of cells per well, allowed estimation of the frequency of Ig-secreting B cells responsive to LPS stimulation and the frequency of Ig-secreting B cells with specific reactivity to a given antigen [70-72]. Tests were chosen according to the type of variable and indicated in each result. Results with $P > 0.05$ were considered significant.

Acknowledgments

We extend our gratitude to all study participants for their time and contribution to our research. We thank the members of the Laboratório de Instrumentação Nuclear (CT - UFRJ) for their assistance with cell irradiation; the Unidade Multiusuário de Citometria - IMPG (CCS/UFRJ) team for their support with the MoFlo sorter (Dako Cytomation) and technical assistance; Ronaldo Rocha (LAGIIVIR, IMPG – UFRJ) for technical assistance. We are grateful to Dr. Garnett Kelsoe (Duke University, Durham, NC) for generously providing the NB21 feeder cells and to Victor Ramos (Laboratory of Molecular Immunology, The Rockefeller University) for sharing the human V gene database and supporting the V gene segment analysis. We hank Professor Pedro Moreno Pimentel-Coelho from the Laboratório de Neuropatologia Experimental (LINE - UFRJ). We also thank all the GIISER-Brazil members for their contributions.

This work was partially funded by GIISER-Brazil/BMGF to ACB and AMV; the Stavros Niarchos Foundation Institute at Rockefeller University (SNIFRU) to GDV and AMV; and the Brazilian research funding agencies: Fundação de Amparo à Pesquisa do Estado do Rio de Janeiro (FAPERJ), Conselho Nacional de Desenvolvimento Científico e Tecnológico (CNPq), Coordenação de Aperfeiçoamento de Pessoal de Nível Superior (CAPES), Financiadora de Estudos e Projetos (FINEP) and Fundação de Amparo à Pesquisa de Minas Gerais (FAPEMIG) [APQ-00501-23, APQ-04025-23, Rede Mineira de Imunobiologicos grant #REDE-00140-16]. L. Conde received a PhD fellowship from FAPERJ. Additional funding was provided by INOVA COVID-19/FIOCRUZ, INCT NeuroImmunomodulation, Rede de ImunoInflamação, and FOCEM/Mercosul to ACB; Instituto Serrapilheira grant to AT; CAPES

(COMBATECovid) and ANRS | Maladies infectieuses émergentes/Inserm grant (MUCOVID-007) grant to MTB; Corona-Ômica -CNPq/FINEP to LJC.

References

1. Phelan, A.L., R. Katz, and L.O. Gostin, *The Novel Coronavirus Originating in Wuhan, China: Challenges for Global Health Governance.* JAMA, 2020. **323**(8): p. 709-710.
2. Yewdell, J.W., *Antigenic drift: Understanding COVID-19.* Immunity, 2021. **54**(12): p. 2681-2687.
3. Kurosaki, T., K. Kometani, and W. Ise, *Memory B cells.* Nat Rev Immunol, 2015. **15**(3): p. 149-59.
4. Moran, I., et al., *Memory B cells are reactivated in subcapsular proliferative foci of lymph nodes.* Nat Commun, 2018. **9**(1): p. 3372.
5. Bernasconi, N.L., E. Traggiai, and A. Lanzavecchia, *Maintenance of serological memory by polyclonal activation of human memory B cells.* Science, 2002. **298**(5601): p. 2199-202.
6. Hou, D., et al., *High-Throughput Sequencing-Based Immune Repertoire Study during Infectious Disease.* Front Immunol, 2016. **7**: p. 336.
7. Tiller, T., et al., *Efficient generation of monoclonal antibodies from single human B cells by single cell RT-PCR and expression vector cloning.* J Immunol Methods, 2008. **329**(1-2): p. 112-24.
8. Pinna, D., et al., *Clonal dissection of the human memory B-cell repertoire following infection and vaccination.* Eur J Immunol, 2009. **39**(5): p. 1260-70.
9. Nojima, T., et al., *In-vitro derived germinal centre B cells differentially generate memory B or plasma cells in vivo.* Nat Commun, 2011. **2**: p. 465.
10. Vale, A.M., et al., *A rapid and quantitative method for the evaluation of V gene usage, specificities and the clonal size of B cell repertoires.* J Immunol Methods, 2012. **376**(1-2): p. 143-9.
11. Collins, L.S. and K. Dorshkind, *A stromal cell line from myeloid long-term bone marrow cultures can support myelopoiesis and B lymphopoiesis.* J Immunol, 1987. **138**(4): p. 1082-7.
12. Kuraoka, M., et al., *Complex Antigens Drive Permissive Clonal Selection in Germinal Centers.* Immunity, 2016. **44**(3): p. 542-552.
13. Andersson, J., O. Sjoberg, and G. Moller, *Mitogens as probes for immunocyte activation and cellular cooperation.* Transplant Rev, 1972. **11**: p. 131-77.
14. Adzavon, Y.M., et al., *TLR7 and TLR8 agonist resiquimod (R848) differently regulates MIF expression in cells and organs.* Cytokine, 2017. **97**: p. 156-166.
15. Nguyen, L.H., et al., *Risk of COVID-19 among frontline healthcare workers and the general community: a prospective cohort study.* medRxiv, 2020.
16. Hoffmann, M., et al., *SARS-CoV-2 Cell Entry Depends on ACE2 and TMPRSS2 and Is Blocked by a Clinically Proven Protease Inhibitor.* Cell, 2020. **181**(2): p. 271-280 e8.
17. Chi, X., et al., *A neutralizing human antibody binds to the N-terminal domain of the Spike protein of SARS-CoV-2.* Science, 2020. **369**(6504): p. 650-655.
18. Diaz-Salinas, M.A., et al., *Single-molecule imaging reveals allosteric stimulation of SARS-CoV-2 spike receptor binding domain by host sialic acid.* Sci Adv, 2024. **10**(29): p. eadk4920.
19. Voss, W.N., et al., *Prevalent, protective, and convergent IgG recognition of SARS-CoV-2 non-RBD spike epitopes.* Science, 2021. **372**(6546): p. 1108-1112.
20. Agudelo, M., et al., *Plasma and memory antibody responses to Gamma SARS-CoV-2 provide limited cross-protection to other variants.* J Exp Med, 2022. **219**(9).
21. Robbiani, D.F., et al., *Convergent antibody responses to SARS-CoV-2 in convalescent individuals.* Nature, 2020. **584**(7821): p. 437-442.
22. Zost, S.J., et al., *Rapid isolation and profiling of a diverse panel of human monoclonal antibodies targeting the SARS-CoV-2 spike protein.* Nat Med, 2020. **26**(9): p. 1422-1427.
23. Wang, Y., et al., *A large-scale systematic survey reveals recurring molecular features of public antibody responses to SARS-CoV-2.* Immunity, 2022. **55**(6): p. 1105-1117 e4.

24. Lima, N.S., et al., *Primary exposure to SARS-CoV-2 variants elicits convergent epitope specificities, immunoglobulin V gene usage and public B cell clones.* Nat Commun, 2022. **13**(1): p. 7733.
25. He, W.T., et al., *Targeted isolation of diverse human protective broadly neutralizing antibodies against SARS-like viruses.* Nat Immunol, 2022. **23**(6): p. 960-970.
26. Yuan, M., et al., *Structural basis of a shared antibody response to SARS-CoV-2.* Science, 2020. **369**(6507): p. 1119-1123.
27. Cao, Y., et al., *Potent Neutralizing Antibodies against SARS-CoV-2 Identified by High-Throughput Single-Cell Sequencing of Convalescent Patients' B Cells.* Cell, 2020. **182**(1): p. 73-84 e16.
28. Clark, S.A., et al., *SARS-CoV-2 evolution in an immunocompromised host reveals shared neutralization escape mechanisms.* Cell, 2021. **184**(10): p. 2605-2617 e18.
29. Kim, S.I., et al., *Stereotypic neutralizing V(H) antibodies against SARS-CoV-2 spike protein receptor binding domain in patients with COVID-19 and healthy individuals.* Sci Transl Med, 2021. **13**(578).
30. Tan, T.J.C., et al., *Sequence signatures of two IGHV3-53/3-66 public clonotypes to SARS-CoV-2 receptor binding domain.* bioRxiv, 2021.
31. Yuan, M., et al., *Recognition of the SARS-CoV-2 receptor binding domain by neutralizing antibodies.* Biochem Biophys Res Commun, 2021. **538**: p. 192-203.
32. Zhang, Q., et al., *Potent and protective IGHV3-53/3-66 public antibodies and their shared escape mutant on the spike of SARS-CoV-2.* Nat Commun, 2021. **12**(1): p. 4210.
33. Briney, B., et al., *Commonality despite exceptional diversity in the baseline human antibody repertoire.* Nature, 2019. **566**(7744): p. 393-397.
34. Yuuki, H., et al., *B cell receptor repertoire abnormalities in autoimmune disease.* Front Immunol, 2024. **15**: p. 1326823.
35. Tong, P., et al., *Memory B cell repertoire for recognition of evolving SARS-CoV-2 spike.* Cell, 2021. **184**(19): p. 4969-4980 e15.
36. Shah, H.B., et al., *Insights From Analysis of Human Antigen-Specific Memory B Cell Repertoires.* Front Immunol, 2018. **9**: p. 3064.
37. Abhiraman, G.C., et al., *A structural blueprint for interleukin-21 signal modulation.* Cell Rep, 2023. **42**(6): p. 112657.
38. Beckers, L., V. Somers, and J. Fraussen, *IgD(-)CD27(-) double negative (DN) B cells: Origins and functions in health and disease.* Immunol Lett, 2023. **255**: p. 67-76.
39. Pabst, O. and E. Slack, *IgA and the intestinal microbiota: the importance of being specific.* Mucosal Immunol, 2020. **13**(1): p. 12-21.
40. Boes, M., *Role of natural and immune IgM antibodies in immune responses.* Mol Immunol, 2000. **37**(18): p. 1141-9.
41. Law, J.L.M., et al., *SARS-COV-2 recombinant Receptor-Binding-Domain (RBD) induces neutralizing antibodies against variant strains of SARS-CoV-2 and SARS-CoV-1.* Vaccine, 2021. **39**(40): p. 5769-5779.
42. McCallum, M., et al., *N-terminal domain antigenic mapping reveals a site of vulnerability for SARS-CoV-2.* Cell, 2021. **184**(9): p. 2332-2347 e16.
43. Thakur, S., et al., *SARS-CoV-2 Mutations and Their Impact on Diagnostics, Therapeutics and Vaccines.* Front Med (Lausanne), 2022. **9**: p. 815389.
44. Harvey, W.T., et al., *SARS-CoV-2 variants, spike mutations and immune escape.* Nat Rev Microbiol, 2021. **19**(7): p. 409-424.
45. Gupta, D., et al., *Structural and functional insights into the spike protein mutations of emerging SARS-CoV-2 variants.* Cell Mol Life Sci, 2021. **78**(24): p. 7967-7989.
46. Wec, A.Z., et al., *Broad neutralization of SARS-related viruses by human monoclonal antibodies.* Science, 2020. **369**(6504): p. 731-736.
47. Barnes, C.O., et al., *Structures of Human Antibodies Bound to SARS-CoV-2 Spike Reveal Common Epitopes and Recurrent Features of Antibodies.* Cell, 2020. **182**(4): p. 828-842 e16.

48. Alvim, R.G.F., et al., *From a recombinant key antigen to an accurate, affordable serological test: Lessons learnt from COVID-19 for future pandemics.* Biochem Eng J, 2022. **186**: p. 108537.
49. Qing, E., et al., *Dynamics of SARS-CoV-2 Spike Proteins in Cell Entry: Control Elements in the Amino-Terminal Domains.* mBio, 2021. **12**(4): p. e0159021.
50. Zhou, P., et al., *Broadly neutralizing anti-S2 antibodies protect against all three human betacoronaviruses that cause deadly disease.* Immunity, 2023. **56**(3): p. 669-686 e7.
51. Sheward, D.J., et al., *Neutralisation sensitivity of the SARS-CoV-2 omicron (B.1.1.529) variant: a cross-sectional study.* Lancet Infect Dis, 2022. **22**(6): p. 813-820.
52. Trombetta, J.J., et al., *Preparation of Single-Cell RNA-Seq Libraries for Next Generation Sequencing.* Curr Protoc Mol Biol, 2014. **107**: p. 4 22 1-4 22 17.
53. McDaniel, J.R., et al., *Ultra-high-throughput sequencing of the immune receptor repertoire from millions of lymphocytes.* Nat Protoc, 2016. **11**(3): p. 429-42.
54. Alamyar, E., et al., *IMGT((R)) tools for the nucleotide analysis of immunoglobulin (IG) and T cell receptor (TR) V-(D)-J repertoires, polymorphisms, and IG mutations: IMGT/V-QUEST and IMGT/HighV-QUEST for NGS.* Methods Mol Biol, 2012. **882**: p. 569-604.
55. Retter, I., et al., *VBASE2, an integrative V gene database.* Nucleic Acids Res, 2005. **33**(Database issue): p. D671-4.
56. Soto, C., et al., *High frequency of shared clonotypes in human B cell receptor repertoires.* Nature, 2019. **566**(7744): p. 398-402.
57. Guo, Y., et al., *cAb-Rep: A Database of Curated Antibody Repertoires for Exploring Antibody Diversity and Predicting Antibody Prevalence.* Front Immunol, 2019. **10**: p. 2365.
58. Ivanov, II, et al., *Development of the expressed Ig CDR-H3 repertoire is marked by focusing of constraints in length, amino acid use, and charge that are first established in early B cell progenitors.* J Immunol, 2005. **174**(12): p. 7773-80.
59. Crooks, G.E., et al., *WebLogo: a sequence logo generator.* Genome Res, 2004. **14**(6): p. 1188-90.
60. Kyte, J. and R.F. Doolittle, *A simple method for displaying the hydropathic character of a protein.* J Mol Biol, 1982. **157**(1): p. 105-32.
61. Abanades, B., et al., *ImmuneBuilder: Deep-Learning models for predicting the structures of immune proteins.* Commun Biol, 2023. **6**(1): p. 575.
62. Studer, G., et al., *QMEANDisCo-distance constraints applied on model quality estimation.* Bioinformatics, 2020. **36**(6): p. 1765-1771.
63. Kozakov, D., et al., *The ClusPro web server for protein-protein docking.* Nat Protoc, 2017. **12**(2): p. 255-278.
64. Dolinsky, T.J., et al., *PDB2PQR: expanding and upgrading automated preparation of biomolecular structures for molecular simulations.* Nucleic Acids Res, 2007. **35**(Web Server issue): p. W522-5.
65. Schrödinger, L., & DeLano, W. *PyMOL*. 2020; Available from: Retrieved from http://www.pymol.org/pymol.
66. Honorato, R.V., et al., *The HADDOCK2.4 web server for integrative modeling of biomolecular complexes.* Nat Protoc, 2024. **19**(11): p. 3219-3241.
67. Wrapp, D., et al., *Cryo-EM structure of the 2019-nCoV spike in the prefusion conformation.* Science, 2020. **367**(6483): p. 1260-1263.
68. Xue, L.C., et al., *PRODIGY: a web server for predicting the binding affinity of protein-protein complexes.* Bioinformatics, 2016. **32**(23): p. 3676-3678.
69. Radom, F., A. Pluckthun, and E. Paci, *Assessment of ab initio models of protein complexes by molecular dynamics.* PLoS Comput Biol, 2018. **14**(6): p. e1006182.
70. Fazekas de St, G., *The evaluation of limiting dilution assays.* J Immunol Methods, 1982. **49**(2): p. R11-23.
71. Taswell, C., *Limiting dilution assays for the determination of immunocompetent cell frequencies. I. Data analysis.* J Immunol, 1981. **126**(4): p. 1614-9.

72. Andersson, J., et al., *Clonal growth and maturation to immunoglobulin secretion in vitro of every growth-inducible B lymphocyte.* Cell, 1977. **10**(1): p. 27-34.

Figures and Legends

Figure 1

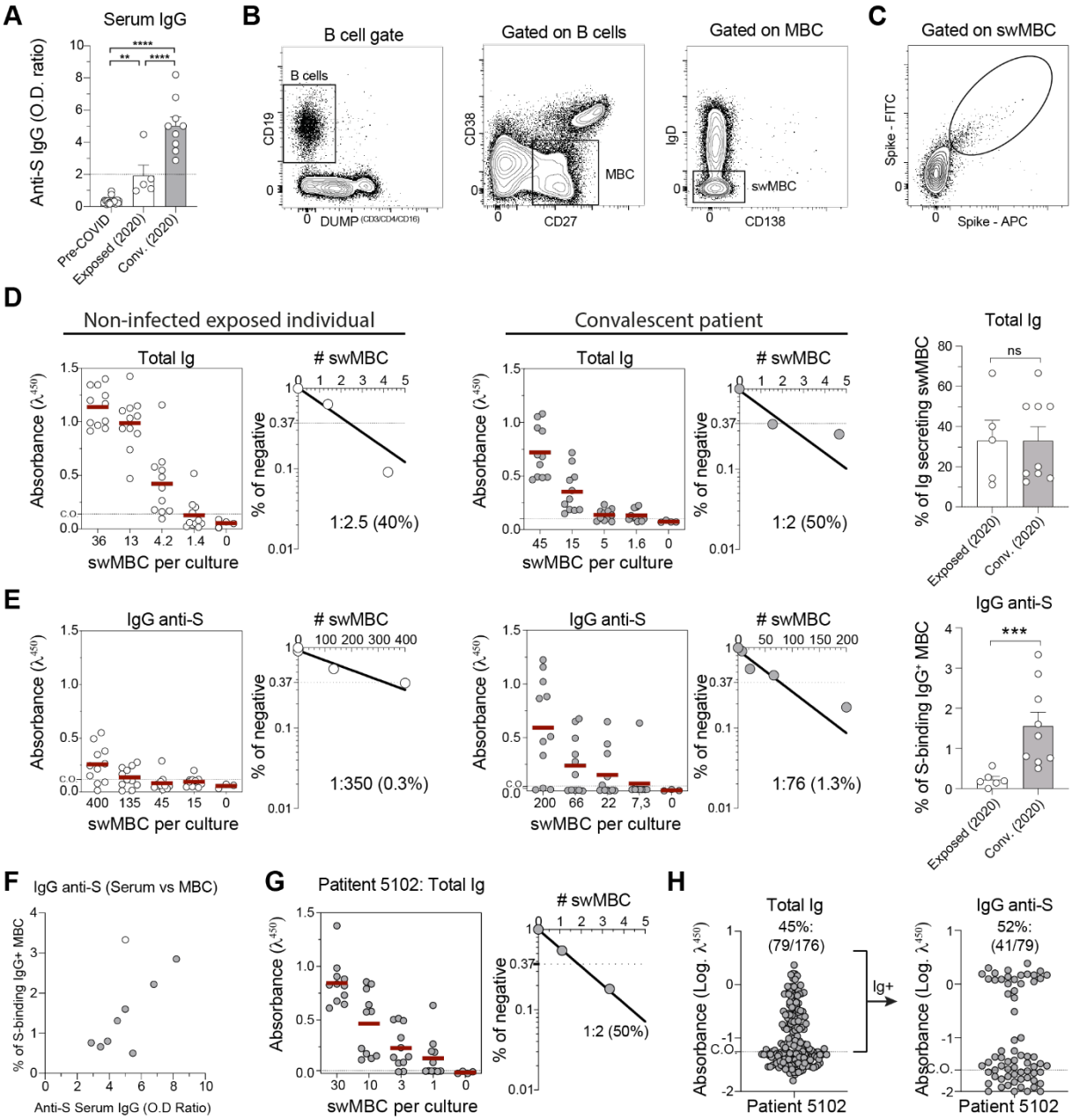

Figure 1: Validation of a culture method for comprehensive and unbiased analysis of the human memory B cell (MBC) repertoire. (A) Serology analysis showing the optical density (OD) ratio of Spike-specific IgG in pre-COVID, negative-exposure, and convalescent patients, assayed by ELISA. Statistical analyses were performed using one-way ANOVA, and Turkey's multiple comparison test. **(B)** Gating strategy for sorting total MBCs and plasma cells. **(C)** Gating strategy for sorting Spike-specific MBCs and plasma cells. **(D)** Limiting dilution assay (LDA) results from negative-exposure and convalescent patients, demonstrating total IgG frequency of responses (one representative patient and in the left a dot plot graph). **(E)** Frequency of Spike-specific responses obtained from the LDA culture of negative-exposure

and convalescent patients (one representative patient and in the left a dot plot graph). Statistical analyses were performed using the unpaired two-tailed Student's t test. **(F)** Correlation between the OD ratio of Spike-specific IgG in serum and the percentage of Spike-specific MBCs identified via flow cytometry. **(G)** LDA results from a convalescent patient, showing the frequency of total IgG responses. **(H)** Percentage of monoclonal antibodies isolated of single cell culture (45%) from patient 5102, showing the 52% are specific to the Wuhan Spike protein, closely matching the total IgG response frequency shown in **(G)**. Significant difference is indicated by asterisk (*, $P < 0.05$; **, $P < 0.01$; (***, $P < 0.001$; ****, $P < 0.0001$). Error bars represent SEM.

Figure 2

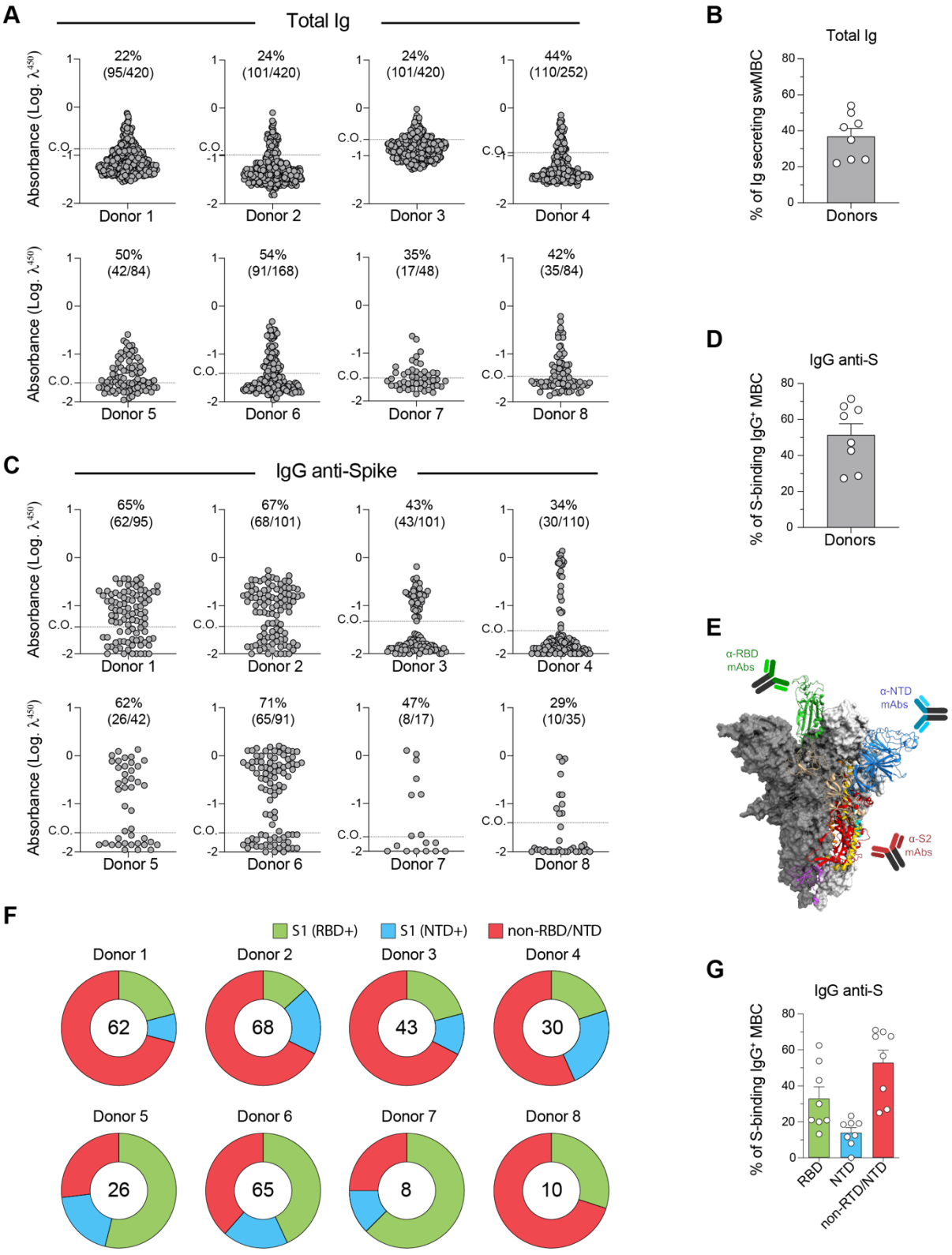

Figure 2: Single-cell cultures (SCCs) for antigen-directed analysis of the Ig repertoire and monoclonal antibody (mAb) isolation. (A) Percentage of mAbs isolated from SCCs across eight vaccinated patients, with antibody-producing cells ranging from 22% to 54%. **(B)** Dot plot illustrating the percentage of mAbs isolated from the eight patients described in **(A)**.

(C) Percentage of mAbs binding to the Wuhan Spike protein, ranging from 29% to 71%, isolated from the eight patients. **(D)** Dot plot showing the percentage of Spike protein-binding mAbs for the eight patients detailed in **(C)**. **(E)** Schematic representation of the Spike protein regions, including the receptor-binding domain (RBD, green), N-terminal domain (NTD, blue), and S2 region (red), which are potential antibody targets. **(F)** Pie charts showing the distribution of mAbs targeting the RBD, NTD, and unknown regions for each of the eight patients. **(G)** Dot plot depicting the percentage of site-specific mAbs binding to the RBD, NTD, and unknown regions for each patient as in **(F)**. Error bars represent SEM.

Figure 3

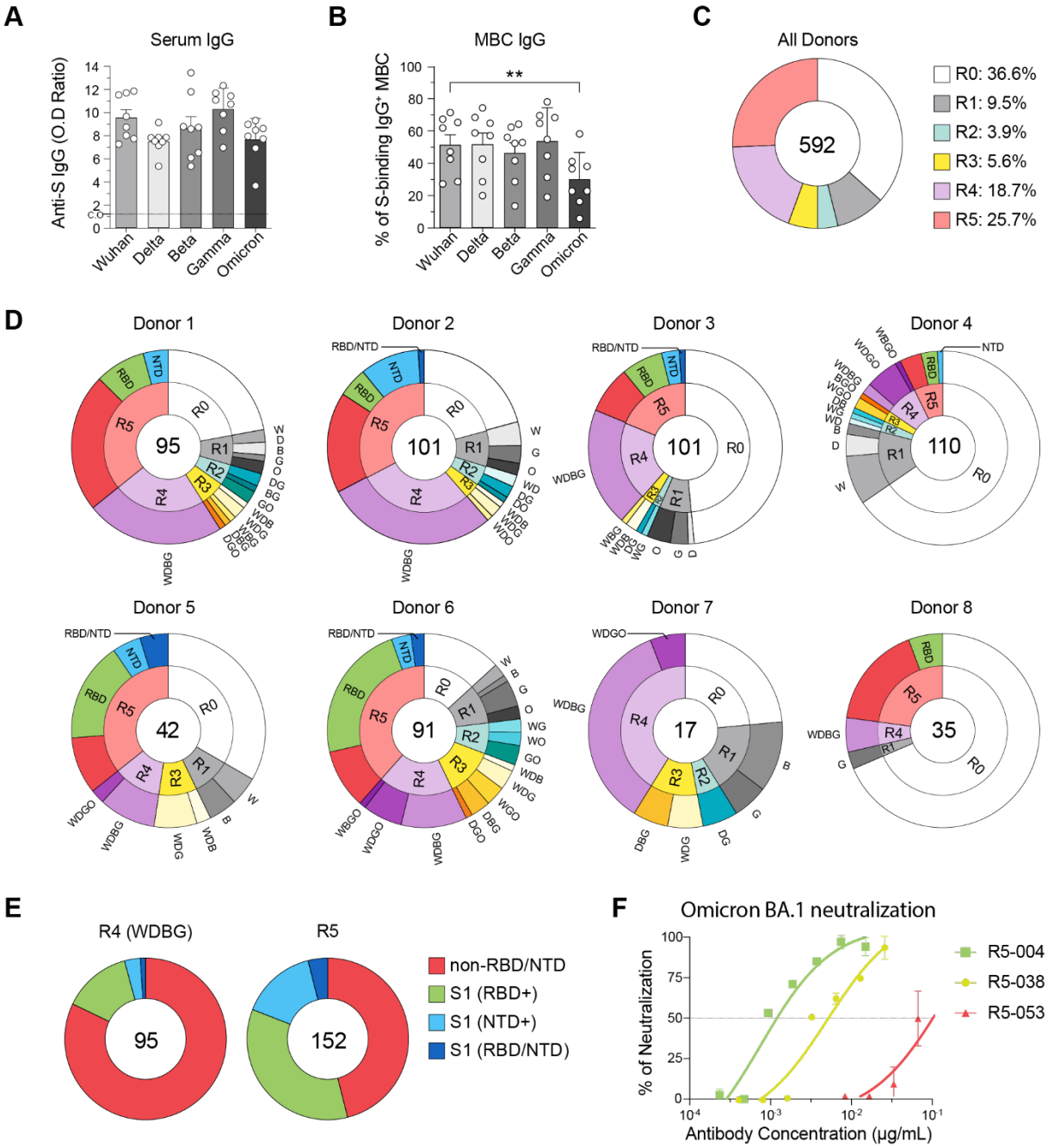

Figure 3: Comparative cross-reactivity analysis of SCC-derived monoclonal antibodies (mAbs) against SARS-CoV-2 spike protein variants. (A) Serum analysis showing Spike-specific antibody responses against variants of concern (VOCs): Wuhan, Delta, Beta, Gamma, and Omicron (BA.2). **(B)** Frequency of IgG+ MBCs that recognized each VOC. S+ MBC cells were sorted, cultured and IgG production was assayed by ELISA. VOC reactivity was also measured by ELISA, through plates coated with Spike proteins from each variant. Statistical analyses were performed using one-way ANOVA, and Turkey's multiple comparison test. Significant difference is indicated by asterisk (**, P < 0.01) **(C)** Monoclonal antibodies isolated from the eight patients, stratified by cross-reactivity levels: R0 (no reactivity), R1 (reactivity to

one variant), R2 (two variants), R3 (three variants), R4 (four variants), and R5 (reactivity to all five tested variants). **(D)** Cross-reactivity profiles for each of the eight patients, detailing the distribution of mAbs by cross-reactivity level and highlighting R5 mAbs, which are further stratified by site-specific binding. R5 mAbs are emphasized due to their greater neutralizing potential. **(E)** Pie charts showing the percentages of R4 mAbs (excluding those non-reactive to Omicron, the most genetically divergent VOC) and R5 mAbs, categorized by specificity to the RBD, NTD, or unknown Spike regions. **(F)** Neutralizing activity of isolated R5 mAbs with site-specific binding to RBD (004 and 038) and putative S2-binding (053).

Figure 4

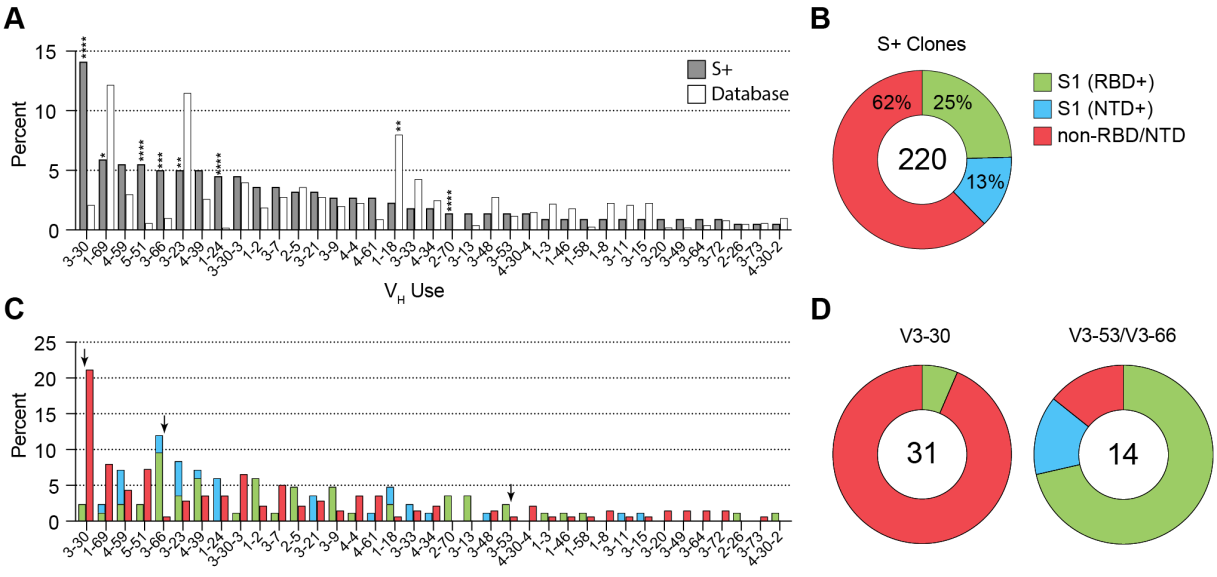

E

Representative convergent clones from different donors and independent datasets

Binding domain	Clone ID	Heavy Chain IGHV	IGHD	IGHJ	CDR-H3	Length	Light Chain IGKV-IGLV	IGKJ-IGLJ	CDR-L3	Length	*Cluster #	Source
RBD	22E1P1D02	IGHV3-66	IGHD2-2	IGHJ6	ARDAQVYGMDV	11	IGKV1-9	IGKJ4	HQLNSDPPAT	10	1 (RBD)	This study
	BD-503	IGHV3-53		IGHJ6	ARDAAVYGIDV	11	IGKV1-39	IGKJ3	QQSYTTPLFT	10		Cao et al, 2020
	22E1P1F08	IGHV3-66	IGHD3-9	IGHJ6	ARDLVVSGMDV	11	IGKV1-9	IGKJ4	QQLNSDPLT	9	1 (RBD)	This study
	C98C7	IGHV3-66	IGHD3-22	IGHJ6	ARDLVVFGMDV	11	IGKV3-20	IGKJ1	QHYGSSP-T	8		Tong et al, 2021
	23E1P2E01	IGHV1-58	IGHD2-15	IGHJ3	AAPSCSGGSCYDGFNI	16	IGKV3-20	IGKJ1	QQYGGTTGWT	10	3 (RBD)	This study
	MnC5t2p1_G1	IGHV1-58	IGHD2-15	IGHJ3	AAPRCSGGSCYDGFDI	16	IGKV3-20	IGKJ1	QQYG-SSPWT	9		Kreer et al, 2020
	CV3-1	IGHV1-58	IGHD2-15	IGHJ3	AAPSCSGGRCYDGFDI	16	IGKV3-20	IGKJ1	QQYG-TSPWT	9		Jennewein et al, 2021
	23E1P1E11	IGHV3-66	IGHD3-10	IGHJ6	ARDLMERGGMDV	12	IGLV1-47	IGLJ2	AAWDDTLSGRGV	12	4 (RBD)	This study
	MOD9_P2_IgG_C9-P1369	IGHV3-66	IGHD2-15	IGHJ6	ARDLMEVGGMDV	12	IGLV1-47	IGLJ1	AAWDDSLSG-YV	12		Wang et al, 2021
Non-RBD/NTD Putative S2	22E1P4D02	IGHV3-30-3	IGHD4-23	IGHJ6	ARATTGGYYGMDV	14	IGKV1-39	IGKJ2	QQSYTTPYT	9	6 (S2)	This study
	DH1202	IGHV3-30		IGHJ6	ARAYSGGYYGMDV	14	IGKV1-39	IGKJ2	QQSY-SLHS	8		Li et al, 2021
	22E1P4B09	IGHV3-30-3	IGHD3-22	IGHJ6	ARATRGSYYGMDV	14	IGKV1-39	IGKJ2	QQGYSGPYT	9	6 (S2)	This study
	DH1149	IGHV3-30		IGHJ6	ARATRGSYYGMDV	14	IGKV1-39	IGKJ3	QQSYSTEFT	9		Li et al, 2021
	22E1P2E08	IGHV3-30	IGHD3-10	IGHJ4	AKPGAANYYSSFDY	14	IGKV3-20	IGKJ2	QQYGSS--YT	8	9 (S2)	This study
	ADI-60708	IGHV3-30	IGHD1-26	IGHJ4	AKGYGGNYYSAFDY	14	IGKV3D-15		QQYNNWPPNT	10		Sakharkar et al, 2021
	22E1P1B05	IGHV3-30	IGHD3-22	IGHJ4	ARVRGGNYGGA-FDY	14	IGLV3-21	IGLJ2	QVWDRSG-DPDVV	12	9 (S2)	This study
	COV2-2248	IGHV3-30	IGHD4-17	IGHJ4	ARDSGGNYGDSYFDY	15	IGLV3-25	IGLJ3	QSVDRSGTYFNWV	13		Zost et al, 2020
	22E1P3D10	IGHV4-59	NoD	IGHJ5	ARGFDP	6	IGKV3-20	IGKJ1	HQYGSSLTWT	10	10 (S2)	This study
	PDI_124	IGHV4-59		IGHJ5	ARGFDP	6	IGKV3-20	IGKJ1	QQYGSSLRWT	10		Wheatley et al, 2021
	22E1P3F12	IGHV3-7	IGHD6-13	IGHJ4	ASLYSGSWNFDY	12	IGLV3-1	IGLJ3	QAWGSSTGV	9	18 (S2)	This study
	COV2-2406	IGHV3-7	IGHD6-13	IGHJ4	ARLGRSSWNFDY	12	IGLV3-1	IGLJ3	QAWDSSTGV	9		Zost et al, 2020

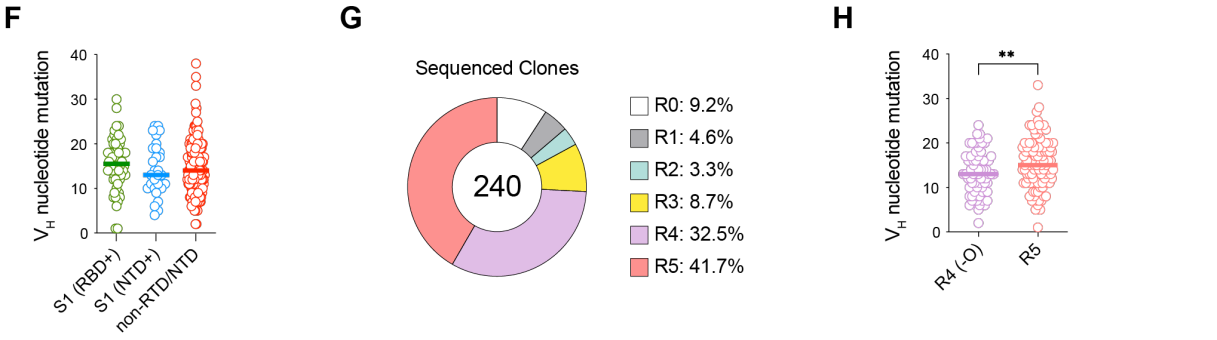

Figure 4: Immunoglobulin repertoire features and convergent V region rearrangements. (**A**) Frequency distribution of IGHV from clones isolated in the current study (gray bars) was compared to the frequency observed in healthy patients' dataset (white bars). Statistical significance determined by two-sided binomial test with unequal variance. (**B**) Pie chart showing the percentage of S specific isolated antibodies that bind RBD, NTD or neither. The total number of antibodies tested is in the middle of the chart. RBD-/NTD- clones are likely to

be S2 binding clones. (**C**) V_H usage distribution for clones that bind RBD, NTD or neither. (**D**) Pie charts displaying the percentage of RBD, NTD or RBD-/NTD- binding clones in V3-30 or V3-53/ V3-66 clones. **(E)** Representative convergent antibody clusters. Clones that share 80% of CDRH3 identity as well as VH/VL usage with previously described clones that fall into clusters defined by Wang and colleagues. **(F)** Number of mutations detected in VH genes per clones that bind RBD, NTD or neither. **(G)** Pie chart with the total number of sequenced clones and the percentual distribution for VOC binding, from 0 variants (R0) to all five (R5). (H) Comparisons in V_H mutations detected per clones that bind four (R4) and five (R5) variants. Statistical analyses were performed using the unpaired two-tailed Student's t test. Significant differences are denoted by asterisks (*, $P < 0.05$; **, $P < 0.01$; ****, $P < 0.0001$).

Figure 5

A

Selected clones for scaleup production

		Heavy Chain					Light Chain				
Binding domain	**Clone ID**	IGHV	IGHJ	CDR-H3	Length	SHM	IGKV-IGLV	IGKJ-IGLJ	CDR-L3	Length	SHM
RBD	LBL01	IGHV3-53	IGHJ6	**ARGGGMGTYGMDV**	13	8	IGKV1-9	IGKJ3	**QHLDSYPQGFT**	11	2
	LBL02	IGHV3-66	IGHJ3	**ARDVADAFDI**	10	18	IGKV1-9	IGKJ2	**QQLNSYPPYT**	10	8

B

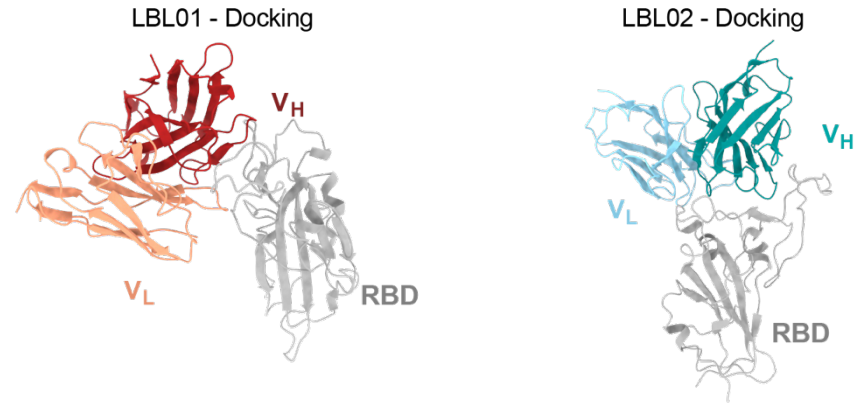

C

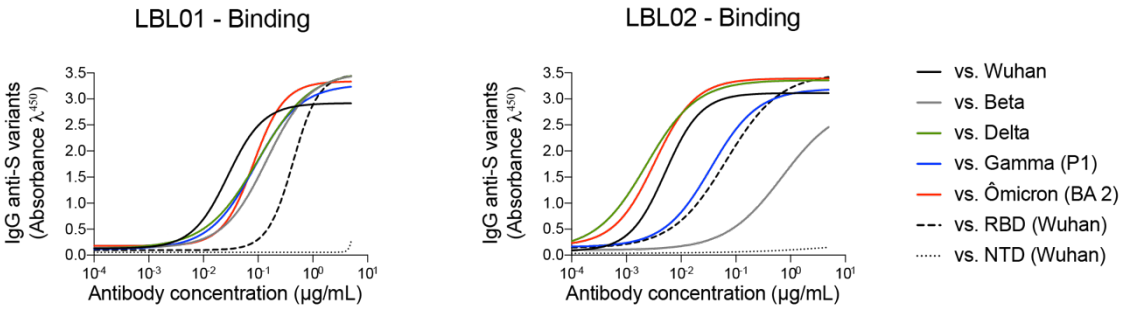

D

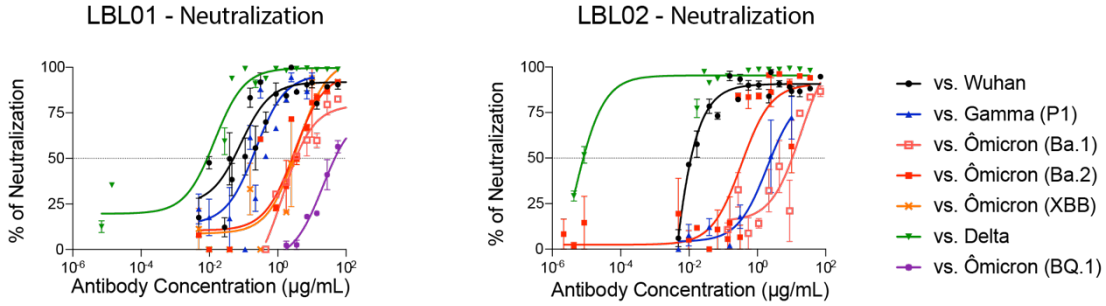

Figure 5: Neutralizing potential of two selected RBD-targeting public clones. (A) Heavy and light chain CDR3 sequences of two public clones (LBL01 and LBL02) characterized by ELISA as RBD binders. **(B)** Computational docking of each clone, showing the potential RBD binding site for each. **(C)** LBL01 and LBL02 antibodies were produced and tested in ELISA against five VOCs, as well as RBD and NTD domains. **(D)** Pseudovirus neutralization assay for both clones, confirming that the broader specificity of LBL02 is also functionally reflected in its stronger neutralization capability

Supplementary material

Supplementary Figure 1

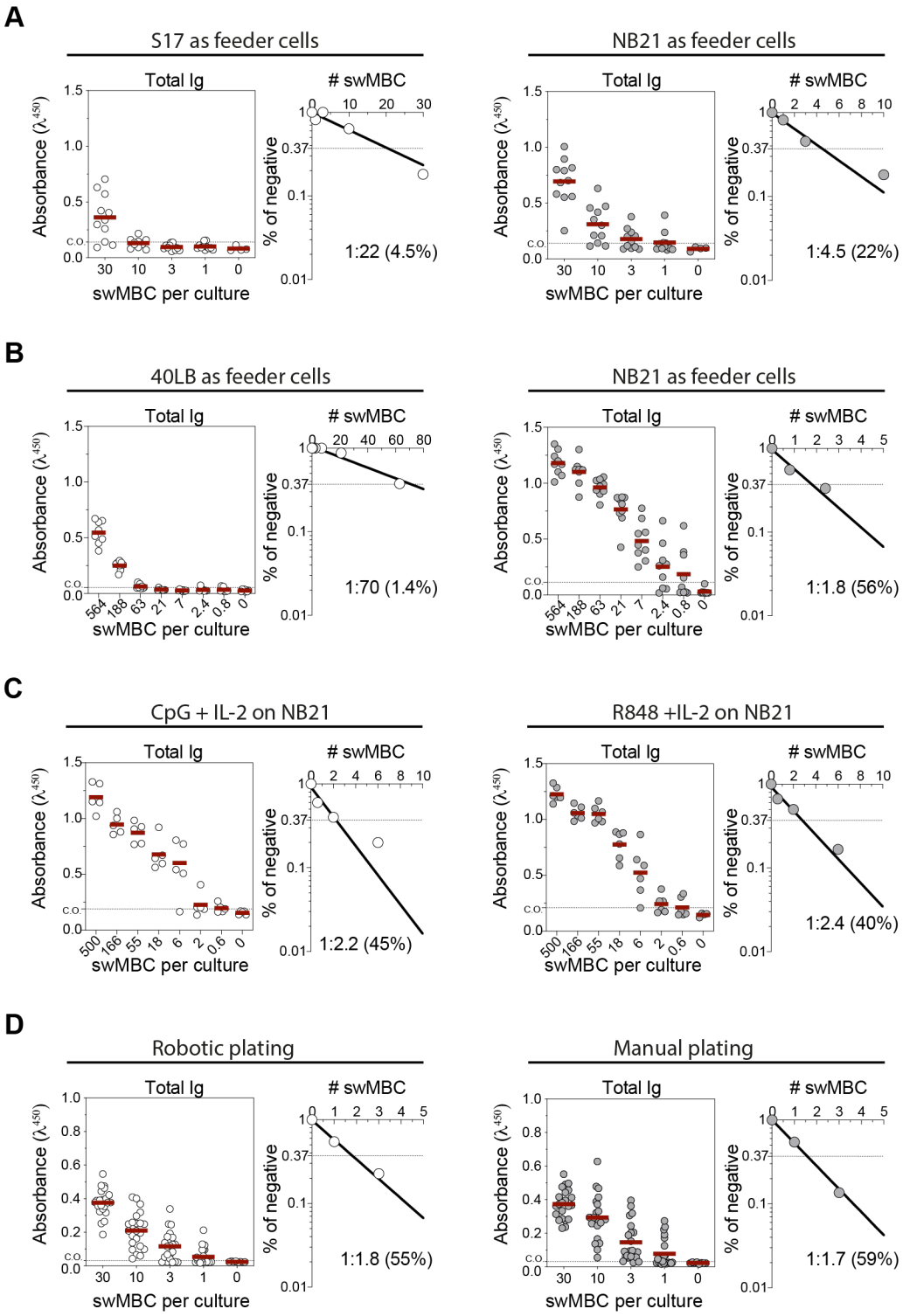

Suppl. Figure 1: Establishing effective culture conditions for *in vitro* expansion of human memory B cell. (A) Frequency of responding MBCs co-cultivated with NB21 feeder cells, S17 and **(B)** hNB40L feeder cells. Decreasing number of B cells were sorted and Ig secretion was assessed by ELISA. In accordance with Poisson distribution, the frequency of

responding cells was calculated as the inverse of the cell density in which 37% of wells did not show detectable levels of Ig (ie, negative cultures). **(C)** Comparison of polyclonal stimuli efficacy using CpG and R848. **(D)** Comparison of responding cells using manual cell plating with automated cell plating with a robotic system integrated into the sorting device.

Supplementary Figure 2

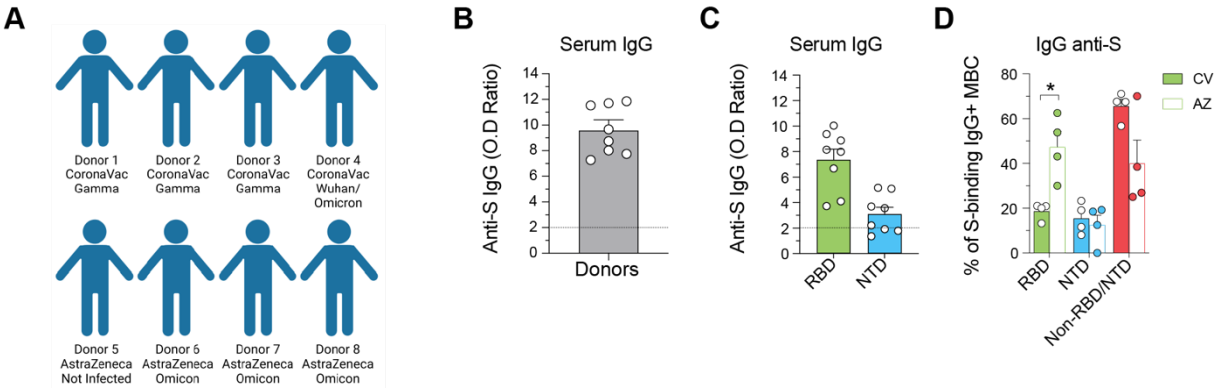

Suppl. Figure 2: Vaccination and infection history of patients used for monoclonal antibody isolation. (A) Schematic representation of the vaccination and infection history for the eight patients from whom monoclonal antibodies were isolated. **(B)** OD ratio of total IgG specific to the Spike protein in the serum of the eight donors. **(C)** O.D. ratio of IgG specific to the RBD and NTD regions in the serum of the eight donors. **(D)** Percentage of Spike-specific antibodies from serum of each patient categorized by binding to the RBD, NTD, and unknown regions. Data are stratified by the type of vaccine administered to the patients: CoronaVac (CV), filled bars, or AstraZeneca (AZ), empty bars. Statistical analyses were performed using the unpaired two-tailed Student's t test. Significant difference is indicated by asterisk (*, $P < 0.05$; **, $P < 0.01$; (***, $P < 0.001$; ****, $P < 0.0001$). Error bars represent SEM.

Supplementary Figure 3

Suppl. Figure 3: Cross-reactivity levels of mAbs evaluated by ELISA. Heatmap showing the binding intensity of monoclonal antibodies (mAbs) to variants of concern (VOCs) in ELISA assays. **(A)** R5 clones were ranked based on their O.D. (optical density) ratio values in the ELISA assay for Wuhan Spike and **(B)** Omicron Spike. Clones marked with an arrow were selected for pseudoneutralization assay.

Supplementary Figure 4

A

ELISA-tested binding position: RBD

22E1P1D02
Binding domain: RBD
CDRH3 AA length and sequence:
11/ ARDAQVYGMDV
V gene usage: IGHV3-66/ IGKV1-9
Binding energy: -11.3 kcal/mol
Buried surface area: 2321.7 +/- 112.4
Cluster size: 40
Z-score: -1.6

22E1P1F08
Binding domain:RBD
CDRH3 AA length and sequence:
11/ ARDLVVSGMDV
V gene usage: IGHV3-66/ IGKV1-9
Binding energy: -10.4 kcal/mol
Buried surface area: 2105.4 +/- 17.3
Cluster size: 161
Z-score: -1.4

B

Putative binding position: S2

22E1P3D10
Binding domain: S2
CDRH3 AA length and sequence:
6 / ARGFDP
V gene usage: IGHV4-59/ IGKV3-20
Binding energy: -11.4 kcal/mol
Buried surface area: 2800.4 +/-180.2
Cluster size: 116

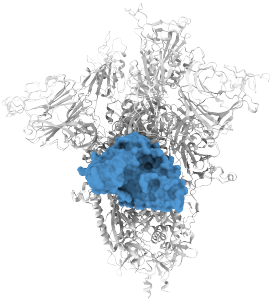

22E1P2E08
Binding domain:S2
CDRH3 AA length and sequence:
14/ AKPGAANYYSSFDY
V gene usage: IGHV3-30/ IGKV3-20
Binding energy: -13.0 kcal/mol
Buried surface area: 2571.6 +/- 59.2
Cluster size: 99

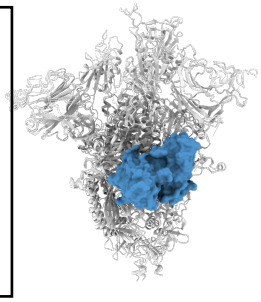

22E1P3F12
Binding domain:S2
CDRH3 AA length and sequence:
12/ ASLYSGSWNFDY
V gene usage: IGHV3-7/ IGLV3-1
Binding energy: -11.2 kcal/mol
Buried surface area: 2071.7 +/- 75.8
Cluster size: 97

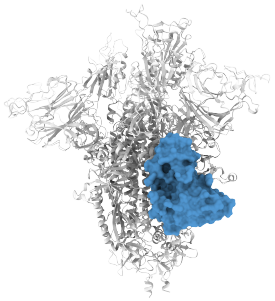

22E1P1B05
Binding domain:S2
CDRH3 AA length and sequence:
14/ ARVRGGNYGGAFDY
V gene usage: IGHV3-30/ IGLV3-21
Binding energy: -8.0 kcal/mol
Buried surface area: 2592.6 +/- 201.6
Cluster size: 71

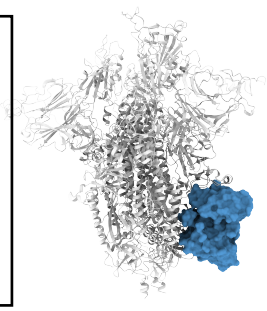

Suppl. Figure 4: *In silico* analysis of antibody binding. (A) Driven docking data of the two selected RBD-binding clones. **(B)** Driven docking data of selected RBD-/NTD-, putative S2 binding clones, that shared CDRH3 sequence homology and V_H gene segments with clustered clones that are known to bind S2 domain.

Supplementary Figure 5

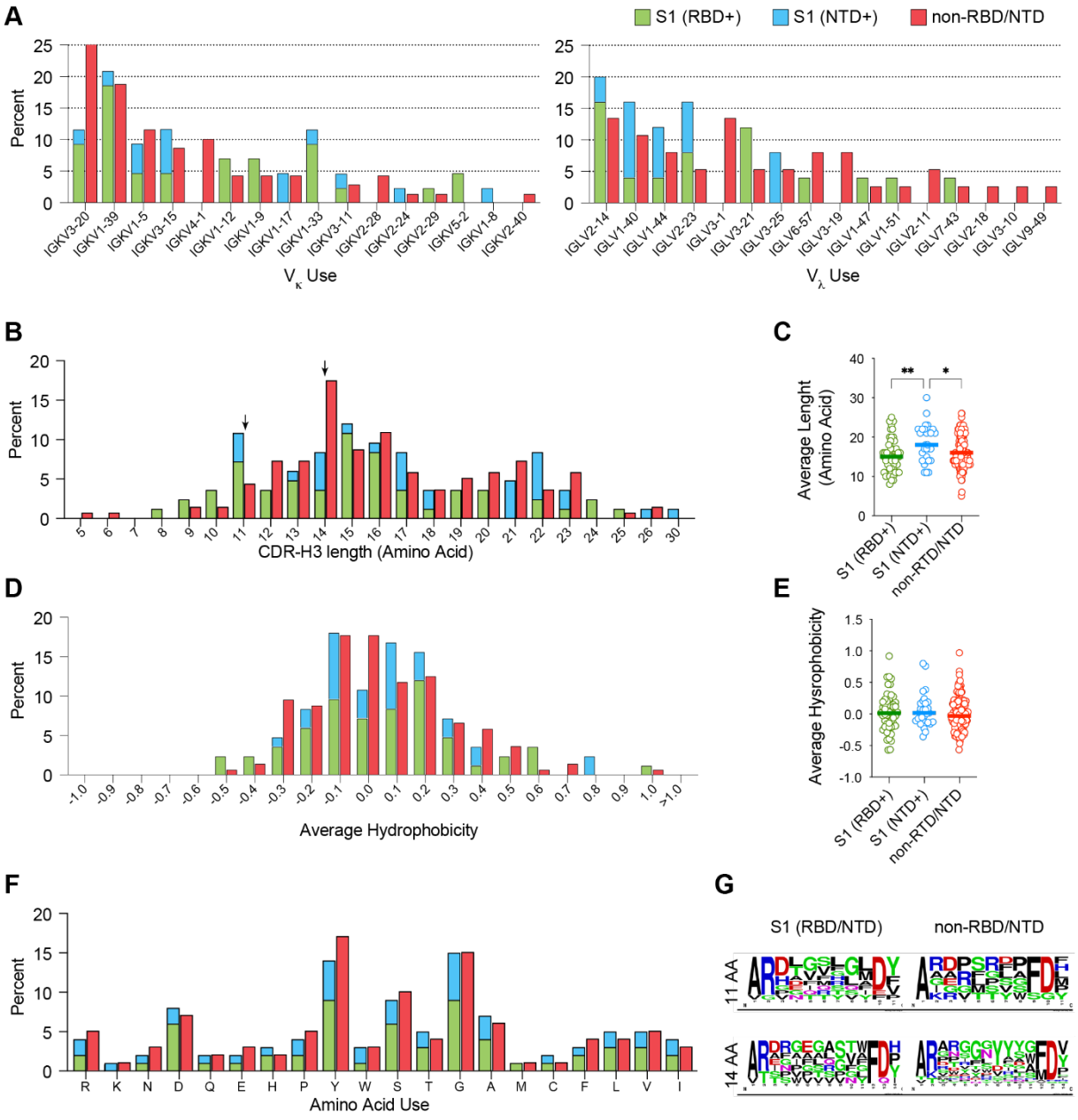

Suppl. Figure 5: IGKV and IGLV gene usage and CDR-H3 repertoire analysis. (**A**) The distribution of CDRL3 V gene usage in Kappa and Lambda alleles was determined for RBD, NTD or RBD-/NTD- S binding clones. **(B-C)** CDRH3 amino acid length distribution **(B)** and average length **(B)** for RBD, NTD or RBD-/NTD- S binding clones. Statistical analyses were performed using one-way ANOVA, and Turkey's multiple comparison test. Significant difference is indicated by asterisk (*, P < 0.05; **, P < 0.01). **(D-E)** CDR-H3 average hydrophobicity index variation **(D)** and average hydrophobicity distribution **(E)** for RBD, NTD or RBD-/NTD- S binding clones. **(F)** Amino acid usage in CDRH3 of the assessed clones. **(G)** Logo plot for amino acid usage in clones that bind RBD/NTD or not, with CDRH3 with length of 11 and 14 amino acids.

Supplementary Table 1: Summary of site-specific and cross-reactive single cell cloning cultures

Supplementary Table 1: Summary of SCC cross-reactivity

Total SCCs per donor		Donor 1 (n = 420)		Donor 2 (n = 420)		Donor 3 (n = 420)		Donor 4 (n = 252)		Donor 5 (n = 84)		Donor 6 (n =168)		Donor 7 (n =48)		Donor 8 (n =84)		Total (n=1896)	
Immunoreactivity		#	%	#	%	#	%	#	%	#	%	#	%	#	%	#	%	#	%
Total Ig secreting SCCs		95	100.0	101	100.0	101	100.0	110	100.0	42	100.0	91	100.0	17	100.0	35	100.0	592	100.0
Spike +	Wuhan (W)	62	65.3	68	67.3	43	42.6	30	27.3	26	61.9	65	71.4	8	47.1	10	28.6	312	52.7
Spike region	RBD (W)	13	21.0	9	13.2	9	20.9	6	20.0	14	53.8	28	43.1	5	62.5	3	30.0	87	27.9
	NTD (W)	5	8.1	13	19.1	5	11.6	7	23.3	5	19.2	12	18.5	1	12.5	0	0.0	48	15.4
	non-RBD/NTD	44	71.0	46	67.6	29	67.4	17	56.7	7	26.9	25	38.5	2	25.0	7	70.0	177	56.7
VOCs	Delta (D)	65	68.4	75	74.3	43	42.6	22	20.0	24	57.1	59	64.8	10	58.8	10	28.6	308	52.0
	Beta (B)	61	64.2	63	62.4	42	41.6	15	13.6	22	52.4	51	56.0	9	52.9	10	28.6	273	46.1
	Gamma G)	66	69.5	69	68.3	45	44.6	21	19.1	23	54.8	71	78.0	11	64.7	11	31.4	317	53.5
	Omicron (O)	39	41.1	37	36.6	23	22.8	18	16.4	16	38.1	53	58.2	1	5.9	8	22.9	195	32.9
Cross-reactivity level																			
R0		21	22.1	21	20.8	49	48.5	72	65.5	14	33.3	12	13.2	4	23.5	24	68.6	217	36.7
R1, R2, R3, R4, R5		74	77.9	80	79.2	52	51.5	38	34.5	28	66.7	79	86.8	13	76.5	11	31.4	375	63.3
R1		7	7.4	9	8.9	8	7.9	15	13.6	4	9.5	9	9.9	3	17.6	1	2.9	56	9.5
R1: VOCs	W	2	2.1	0	0.0	0	0.0	9	8.2	2	4.8	2	2.2	0	0.0	0	0.0	15	2.5
	D	2	2.1	4	4.0	1	1.0	4	3.6	0	0.0	0	0.0	0	0.0	0	0.0	11	1.9
	B	1	1.1	0	0.0	0	0.0	2	1.8	2	4.8	1	1.1	2	11.8	0	0.0	8	1.4
	G	0	0.0	3	3.0	3	3.0	0	0.0	0	0.0	4	4.4	1	5.9	1	2.9	12	2.0
	O	2	2.1	2	2.0	4	4.0	0	0.0	0	0.0	2	2.2	0	0.0	0	0.0	10	1.7
R2		5	5.3	5	5.0	2	2.0	3	2.7	0	0.0	7	7.7	1	5.9	0	0.0	23	3.9
R2: VOC combinations	WD	0	0.0	2	2.0	0	0.0	1	0.9	0	0.0	0	0.0	0	0.0	0	0.0	3	0.5
	WB	0	0.0	0	0.0	0	0.0	0	0.0	0	0.0	0	0.0	0	0.0	0	0.0	0	0.0
	WG	0	0.0	0	0.0	1	1.0	1	0.9	0	0.0	2	2.2	0	0.0	0	0.0	4	0.7
	WO	0	0.0	0	0.0	0	0.0	0	0.0	0	0.0	2	2.2	0	0.0	0	0.0	2	0.3
	DB	0	0.0	0	0.0	0	0.0	1	0.9	0	0.0	0	0.0	0	0.0	0	0.0	1	0.2
	DG	2	2.1	2	2.0	1	1.0	0	0.0	0	0.0	0	0.0	1	5.9	0	0.0	6	1.0
	DO	0	0.0	1	1.0	0	0.0	0	0.0	0	0.0	0	0.0	0	0.0	0	0.0	1	0.2
	BG	1	1.1	0	0.0	0	0.0	0	0.0	0	0.0	0	0.0	0	0.0	0	0.0	1	0.2
	BO	0	0.0	0	0.0	0	0.0	0	0.0	0	0.0	0	0.0	0	0.0	0	0.0	0	0.0
	GO	2	2.1	0	0.0	0	0.0	0	0.0	0	0.0	3	3.3	0	0.0	0	0.0	5	0.8
R3		6	6.3	4	4.0	3	3.0	3	2.7	4	9.5	11	12.1	2	11.8	0	0.0	33	5.6
R3: VOC combinations	WDB	1	1.1	1	1.0	2	2.0	0	0.0	1	2.4	1	1.1	0	0.0	0	0.0	6	1.0
	WDG	2	2.1	2	2.0	0	0.0	0	0.0	3	7.1	3	3.3	1	5.9	0	0.0	11	1.9
	WDO	0	0.0	1	1.0	0	0.0	0	0.0	0	0.0	0	0.0	0	0.0	0	0.0	1	0.2
	WBG	1	1.1	0	0.0	1	1.0	0	0.0	0	0.0	0	0.0	0	0.0	0	0.0	2	0.3
	WBO	0	0.0	0	0.0	0	0.0	0	0.0	0	0.0	0	0.0	0	0.0	0	0.0	0	0.0
	WGO	0	0.0	0	0.0	0	0.0	2	1.8	0	0.0	3	3.3	0	0.0	0	0.0	5	0.8
	DBG	1	1.1	0	0.0	0	0.0	0	0.0	0	0.0	3	3.3	1	5.9	0	0.0	5	0.8
	DBO	0	0.0	0	0.0	0	0.0	0	0.0	0	0.0	0	0.0	0	0.0	0	0.0	0	0.0
	DGO	1	1.1	0	0.0	0	0.0	0	0.0	0	0.0	1	1.1	0	0.0	0	0.0	2	0.3
	BGO	0	0.0	0	0.0	0	0.0	1	0.9	0	0.0	0	0.0	0	0.0	0	0.0	1	0.2
R4		22	23.2	29	28.7	20	19.8	9	8.2	5	11.9	17	18.7	7	41.2	2	5.7	111	18.8
R4: VOC combinations	WDBG	22	23.2	29	28.7	20	19.8	2	1.8	4	9.5	10	11.0	6	35.3	2	5.7	95	16.0
	WDBO	0	0.0	0	0.0	0	0.0	0	0.0	0	0.0	0	0.0	0	0.0	0	0.0	0	0.0
	WDGO	0	0.0	0	0.0	0	0.0	6	5.5	1	2.4	6	6.6	1	5.9	0	0.0	14	2.4
	WBGO	0	0.0	0	0.0	0	0.0	1	0.9	0	0.0	1	1.1	0	0.0	0	0.0	2	0.3
	DBGO	0	0.0	0	0.0	0	0.0	0	0.0	0	0.0	0	0.0	0	0.0	0	0.0	0	0.0
R5		34	35.8	33	32.7	19	18.8	8	7.3	15	35.7	35	38.5	0	0.0	8	22.9	152	25.7
Spike region	non-RBD/NTD	22	23.2	17	16.8	8	7.9	4	3.6	4	9.5	9	9.9	0	0.0	6	17.1	70	11.8
	RBD+	8	8.4	5	5.0	7	6.9	3	2.7	7	16.7	21	23.1	0	0.0	2	5.7	53	9.0
	NTD+	4	4.2	10	9.9	3	3.0	1	0.9	2	4.8	3	3.3	0	0.0	0	0.0	23	3.9
	RBD/NTD	0	0.0	1	1.0	1	1.0	0	0.0	2	4.8	2	2.2	0	0.0	0	0.0	6	1.0